FAM83D directs protein kinase CK1α to the mitotic spindle for proper spindle positioning

Luke J. Fulcher[1], Zhengcheng He[2], Lin Mei[2], Thomas J. Macartney[1], Nicola T. Wood[1], Alan R. Prescott[3], Arlene J. Whigham[4], Joby Varghese[1], Robert Gourlay[1], Graeme Ball[3], Rosemary Clarke[4], David G. Campbell[1], Christopher A. Maxwell[2], and Gopal P. Sapkota[1*].

[1]Medical Research Council, Protein Phosphorylation and Ubiquitylation Unit, University of Dundee, Dundee, United Kingdom. [2]Michael Cuccione Childhood Cancer Research Program, British Columbia Children's Hospital, University of British Columbia, Vancouver, Canada.[3]Dundee Imaging Facility, School of Life Sciences, University of Dundee. [4]Flow Cytometry and Sorting Facility, School of Life Sciences, University of Dundee.

* Correspondence and requests for materials should be addressed to: g.sapkota@dundee.ac.uk

Summary:

The concerted action of many protein kinases helps orchestrate the error-free progression through mitosis of mammalian cells. The roles and regulation of some prominent mitotic kinases, such as cyclin-dependent kinases, are well-established. However, these and other known mitotic kinases alone cannot account for the extent of protein phosphorylation that has been reported during mammalian mitosis. Here we demonstrate that CK1α, of the casein kinase 1 family of protein kinases, localises to the spindle and is required for proper spindle-positioning and timely cell division. CK1α is recruited to the spindle by FAM83D, and cells devoid of *FAM83D*, or those harbouring CK1α-binding-deficient *FAM83D*$^{F283A/F283A}$ knockin mutation, display pronounced spindle-positioning defects, and a prolonged mitosis. Restoring *FAM83D* at the endogenous locus in *FAM83D*$^{-/-}$ cells, or artificially delivering CK1α to the spindle in *FAM83D*$^{F283A/F283A}$ cells, rescues these defects. These findings implicate CK1α as new mitotic kinase that orchestrates the kinetics and orientation of cell division.

The prominent mitotic roles for kinases such as cyclin-dependent kinases (CDKs), Aurora kinases, Polo-like kinases (PLKs) and Nima-related kinases (NEKs) have been well-characterised (Archambault & Glover, 2009, Barr, Sillje et al., 2004, Carmena & Earnshaw, 2003, Combes, Alharbi et al., 2017, Fu, Bian et al., 2007, Hochegger, Takeda et al., 2008, Nigg, 2001). However, the role of CK1α in mitosis, if any, remains poorly defined. CK1α belongs to the CK1 family of ser/thr protein kinases that are implicated in diverse roles in a whole plethora of cellular processes, from Wnt signalling to the regulation of circadian rhythms (Knippschild, Gocht et al., 2005). CK1 isoforms can phosphorylate hundreds of proteins in vitro, with a preference for ser/thr residues that conform to either a D/E-X-X-S*/T* or pS/pT-X-X-S*/T* motif (Venerando, Ruzzene et al., 2014). A recent mitotic phosphoproteomic study found that around half of the identified phosphorylation sites conformed to the predicted CK1-consensus phosphorylation motifs (Ly, Whigham et al., 2017), potentially implying a significant role for CK1 catalytic activity in mitotic protein phosphorylation. Yet, there is a lack of definitive evidence regarding whether and how any of the CK1 isoforms, or CK1α in particular, are involved in mitosis.

Regarded as constitutively-active protein kinases, the regulation of CK1 isoforms is critically important, yet poorly understood; especially when considering their participation in multiple, diverse, cellular functions in many, different cellular compartments (Knippschild et al., 2005, Schittek & Sinnberg, 2014). We recently reported that the FAM83 family of poorly characterised proteins act as subcellular anchors for CK1 isoforms through the conserved N-terminal domain of unknown function 1669 (DUF1669) (Fulcher, Bozatzi et al., 2018). Our findings that FAM83 proteins interact and co-localise with different CK1 isoforms offer the tantalising possibility that FAM83 proteins direct CK1 isoforms to specific subcellular compartments, and in doing so, regulate their substrate availability/accessibility. In line with this, we have shown that FAM83G (aka PAWS1) activates Wnt signalling through its association with CK1α (Bozatzi, Dingwell et al., 2018). Here, we sought to investigate the FAM83D protein, and define its physiological role in relation to CK1 isoforms. Although FAM83D (aka CHICA) is poorly characterised, it has been shown to be recruited to the mitotic spindle through its association with the microtubule-

associated protein hyaluronan mediated motility receptor (HMMR, aka RHAMM or CD168) (Connell, Chen et al., 2017, Dunsch, Hammond et al., 2012, Santamaria, Nagel et al., 2008). Unlike the other FAM83 members that appear to associate robustly with CK1α, we found that over-expressed GFP-FAM83D in asynchronous cell extracts interacted rather weakly, yet selectively, with CK1α (Fulcher et al., 2018), suggesting this could be a regulated interaction. Consistent with this, in the course of an unbiased proteomic approach to identify interactors of endogenous FAM83D from both asynchronous and mitotic extracts, we discovered in this study that FAM83D interacts with CK1α only in mitosis. As the kinetics of chromosomal alignment are delayed and the cell division axis is altered following the depletion of *FAM83D* by siRNA, as well as in cells lacking *HMMR* or those derived from *HMMR* knockout mice (Connell et al., 2017, Dunsch et al., 2012, Santamaria et al., 2008), we hypothesised that these phenotypes could be potentially explained by the non-delivery of CK1α to the spindle in the absence of FAM83D or HMMR. Here, we show that the FAM83D-CK1α interaction is critically important for correct and efficient spindle positioning, as well as smooth progression through the cell division cycle.

FAM83D & CK1α interact only in mitosis:

In order to investigate the role of FAM83D at physiological levels, we first generated a *FAM83D* knockout, and an in-frame homozygous knockin of a GFP tag at the C-terminus of the endogenous *FAM83D* gene (*FAM83D*$^{GFP/GFP}$) (Fig. EV1) in U2OS cells with CRISPR/Cas9 gene editing technology, and verified these by Western blotting (Fig. 1A) and DNA sequencing. Given the links between FAM83D and mitosis(Dunsch et al., 2012, Santamaria et al., 2008), we next undertook an unbiased proteomic approach to identify interactors of endogenous FAM83D-GFP from either asynchronous or mitotic *FAM83D*$^{GFP/GFP}$ knockin cell extracts. Mitotic cells were collected by shake-off, following either prometaphase arrest with nocodazole and a brief release into fresh medium to allow them to progress into mitosis, or mitotic arrest with the Eg5 chromokinesin inhibitor S-trityl L-cysteine (STLC), which results in monopolar spindle formation (Skoufias, DeBonis et al., 2006). Mass spectrometric analysis of anti-GFP IPs from both asynchronous and mitotic cell extracts identified several known FAM83D interactors, including HMMR, DYNLL1, and the

transcription factor BACH1(Dunsch et al., 2012, Fulcher et al., 2018, Li, Shiraki et al., 2012) (Fig. 1B), potentially revealing the constitutive FAM83D interactors. Excitingly, the only interactor of FAM83D that was robustly identified from mitotic, but not asynchronous extracts, was CK1α (Fig. 1B). The mitotic interactions observed between FAM83D and CK1α or BACH1 constitute novel findings (Fig. 1C).

We sought to validate the interaction between FAM83D and CK1α at the endogenous level. Endogenous CK1α was detected in anti-GFP immunoprecipitates (IPs) from nocodazole-synchronised mitotic but not asynchronous *FAM83D*$^{GFP/GFP}$ cell extracts (Fig. 1D). CK1δ and ε did not interact with FAM83D but known FAM83D interactors HMMR and DYNLL1 were detected in FAM83D IPs from both asynchronous and mitotic cell extracts, suggesting a constitutive mode of interaction (Fig. 1D). A striking electrophoretic mobility shift of FAM83D was observed in mitosis compared to asynchronous cells, suggesting a potential post-translational modification (PTM) (Fig. 1D). In mitotic extracts collected from *FAM83D*$^{GFP/GFP}$ cells following synchronisation with STLC, endogenous CK1α was also detected in anti-GFP IPs (Fig. 1E). Moreover, in cells that were exposed to either nocodazole or STLC but were non-mitotic (i.e. adherent cells that did not shake-off following drug treatment), no interaction between CK1α and FAM83D was observed (Fig. 1E), ruling out possible drug-dependent stimulation of the CK1α:FAM83D interaction. To rule out the possibility that the GFP tag on FAM83D might influence its interaction with CK1α, we employed the 2G *PAI1* U2OS cell line, which harbours a non-fused GFP tag on the *PAI1* locus (Rojas-Fernandez, Herhaus et al., 2015), as a control. Indeed, anti-GFP IPs from these cells did not co-precipitate CK1α (Fig. 1E). Cell cycle stages in asynchronous and mitotic cells were confirmed by flow cytometry following propidium iodide staining (Fig. 1F). At the endogenous level in wild-type U2OS cells, CK1α was detected in anti-FAM83D IPs only from mitotic but not asynchronous extracts, while FAM83D was identified in both. Neither FAM83D nor CK1α were detected in control IgG IPs (Fig. 1G). The mitotic electrophoretic mobility shift of endogenous FAM83D was also apparent in wild-type U2OS cells (Fig. 1G). Endogenous FAM83D was detected in anti-CK1α IPs only from mitotic but not asynchronous extracts, while CK1α was identified in both (Fig. 1H).

Next, to decipher exactly when FAM83D associates with CK1α during the cell division cycle, we arrested *FAM83D*$^{GFP/GFP}$ cells in G2 using the CDK1 inhibitor RO-3306 (Vassilev, 2006), or in mitosis (M) with STLC shake-off, and lysed at 0 (M), 2 (M), 4 (G1) and 6 (G1) hours after STLC-washout (Fig. 1I). Cell cycle stages were assigned by monitoring the levels of cyclin B1 (high in M) and cyclin A2 (high in G2), as well as flow cytometry (Fig. 1I&J). CK1α was only detected in anti-GFP IPs from the mitotic extracts, but not from G2-arrested, G1, or asynchronous extracts (Fig. 1I). As observed before, FAM83D-GFP displayed a robust mobility shift only in the mitotic samples (Fig. 1I).

FAM83D recruits CK1α to the spindle:

We sought to test whether FAM83D and CK1α interact and co-localise in cells during mitosis. In mitotic *FAM83D*$^{GFP/GFP}$ cells, we observed complete overlapping signals between the FAM83D-GFP fluorescence and endogenous CK1α immunofluorescence (IF) signals on the STLC-induced monopolar mitotic spindles (Fig. 2A, top panel). In wild-type cells, which express *FAM83D* without the GFP-tag, we also observed CK1α on mitotic spindles (Fig. 2A; middle panel). Strikingly, consistent with our hypothesis that FAM83 proteins recruit CK1 isoforms to distinct cellular sites, no CK1α signal was evident on the spindle apparatus in *FAM83D*$^{-/-}$ U2OS cells (Fig. 2A; lower panel), suggesting FAM83D recruits CK1α to the spindle in mitosis. No CK1ε staining was detected at the spindle apparatus in either the wild-type, *FAM83D*$^{-/-}$ or *FAM83D*$^{GFP/GFP}$ cells (Fig. EV2A), highlighting the specificity of the FAM83D:CK1α interaction. HMMR, which is responsible for recruiting FAM83D to the spindle in mitosis (Dunsch et al., 2012), was observed at the spindle in wild-type, *FAM83D*$^{-/-}$ and *FAM83D*$^{GFP/GFP}$ cells (Fig. EV2B).

We previously identified two conserved residues (equivalent to D^{249} and F^{283} of FAM83D) within the conserved polypeptide anchor of CK1 (PACK1; aka DUF1669) domain of FAM83 proteins, that were critical for mediating the FAM83:CK1 interaction(Fulcher et al., 2018). GFP-tagged wild-type *FAM83D* but not F283A or D249A mutants transiently expressed in *FAM83D*$^{-/-}$ cells co-precipitated endogenous CK1α during mitosis (Fig. EV3A). Interestingly, we noted that the mitotic

electrophoretic shift evident for wild-type GFP-FAM83D was absent for the two mutants (Fig. EV3A), suggesting that CK1α binding is required for the mitotic mobility shift evident in FAM83D. To validate these findings at the endogenous level, we generated U2OS knockin cell lines harbouring the F283A mutation on *FAM83D* as well as a GFP tag at the C-terminus (hereafter referred to $FAM83D^{GFP/GFP(F283A)}$, Fig. EV1) using CRISPR/Cas9 and verified homozygous knockins by DNA sequencing. Excitingly, like $FAM83D^{-/-}$ cells, no endogenous CK1α IF signal was detected on the spindles in these cells, while overlapping GFP and CK1α signals were observed in $FAM83D^{GFP/GFP}$ cells (Fig. 2B). However, FAM83D(F283A)-GFP still localised to the mitotic spindle, albeit with relatively less GFP fluorescence intensity compared to FAM83D-GFP (Fig. 2B). Quantification of the CK1α IF signal on the mitotic spindle from these cells corroborated these observations (Fig. 2C). Furthermore, endogenous CK1α was detected only in GFP IPs from mitotic $FAM83D^{GFP/GFP}$ cell extracts but not from mitotic $FAM83D^{-/-}$ or $FAM83D^{GFP/GFP\ (F283A)}$ extracts (Fig. 2D). Identical results were obtained with an independent CRISPR $FAM83D^{GFP/GFP(F283A)}$ knockin clone, further confirming these results (Fig. EV3B & C). To further ascertain whether CK1α recruitment to the spindle was dependent on the FAM83D protein, we employed the Affinity-directed PROtein Missile (AdPROM) system (Fulcher, Hutchinson et al., 2017, Fulcher, Macartney et al., 2016) to efficiently degrade FAM83D-GFP using VHL fused to anti-GFP nanobody (VHL-aGFP.16) (Fig. 2E&F; Fig. EV1). In mitotic $FAM83D^{GFP/GFP}$ cells, and $FAM83D^{GFP/GFP}$ cells expressing VHL or aGFP.16 controls, overlapping GFP fluorescence and endogenous CK1α IF signals were evident, but both signals disappeared from mitotic spindles in mitotic $FAM83D^{GFP/GFP}$ cells expressing the VHL-aGFP.16 AdPROM, which resulted in FAM83D-GFP degradation (Fig. 2F&G).

Finally, we rescued the $FAM83D^{-/-}$ U2OS cells by knocking in a polycistronic cassette, consisting of wild-type *FAM83D* cDNA, an IRES element, GFP reporter and polyadenosine tail, directly downstream of the endogenous *FAM83D* promoter (Fig. 3A, Fig. EV1) and obtained and verified two rescue clones by DNA sequencing and immunoblotting (Fig. 3B). In both clones, we verified that the expression of the FAM83D protein and its mitotic phospho-mobility shift closely mirrored that seen in wild-type cells, however the expression of *FAM83D* in clone 11 was slightly lower than

that observed in clone 6 (Fig. 3B). Next, we verified that both FAM83D (Fig. 3C) and CK1α (Fig. 3D&E) localised to the spindle apparatus in both *FAM83D*-rescue clones similar to that observed in wild-type cells. Finally, we also confirmed that the reinstated *FAM83D* in both clones co-precipitated endogenous CK1α only in mitosis (Fig. 3F).

FAM83D and CK1α in unperturbed cells:

In order to determine endogenous FAM83D and CK1α co-localisation at different phases of mitosis in the absence of any drug-induced cell synchronisation, we first knocked in an mCherry tag onto either the *CSNK1A1* gene (CK1α) or the *CSNK1E* gene (CK1ε) in *FAM83D*$^{GFP/GFP}$ U2OS cells by CRISPR/Cas9 (Fig. EV1), and verified homozygous insertions by immunoblotting and IPs (Fig. EV4A&B), as well as genomic DNA sequencing. After confirming that the mCherry tag did not render CK1α inactive (Fig. EV4C), we performed fluorescence microscopy on these cells. We observed robust overlapping centrosomal and mitotic spindle fluorescence between FAM83D-GFP and mCherry-CK1α from prometaphase all the way to anaphase, with less intense co-fluorescence evident in the latter stages of mitosis (Fig. 3G). In contrast, we did not observe spindle localisation of mCherry-CK1ε, nor co-localisation with FAM83D-GFP (Fig. EV4D), at any stage of mitosis.

FAM83D regulation during cell cycle:

The ~25 kDa electrophoretic mobility shift evident for mitotic FAM83D-GFP collapsed substantially when the GFP IPs were subjected to λ-phosphatase treatment, almost to the level of FAM83D-GFP in asynchronous cells (Fig. 4A), suggesting that this mobility shift was due to phosphorylation. Using the mobility shift as a readout, we investigated FAM83D phosphorylation over the course of a cell division following release after STLC synchronisation. As expected, there was a reduction in levels of cyclin B1 and phospho-histone H3 phosphorylation as cells progressed through mitosis (Chang, Xu et al., 2003, Crosio, Fimia et al., 2002), indicating that cells started exiting mitosis around 2 h after STLC washout (Fig. 4B). Interestingly, concurrent reduction in the levels of both HMMR and phospho-FAM83D were observed, suggesting that both proteins are regulated in a cell cycle-dependent manner (Fig. 4B). Such patterns

in the levels of cell cycle-regulated proteins are often associated with their degradation following mitotic exit, or during metaphase-to-anaphase transition (Chang et al., 2003, Koepp, 2014). Interestingly, the protein levels of CK1α did not change after the STLC washout (Fig. 4B). Considering that both FAM83D and CK1α appear to dissociate from the spindle following the metaphase-to-anaphase transition (Fig. 3F), it appears likely that following FAM83D degradation, CK1α can no longer localise to the spindle, and dissociates into the cytosol. The reduction in FAM83D and HMMR protein levels following STLC washout were blocked with MG132 (Fig. 4C), suggesting that FAM83D and HMMR potentially undergo proteasomal degradation upon mitotic exit. Cyclin B1 levels were also rescued by MG132 treatment (Fig. 4C). As MG132 is also known to inhibit the metaphase-to-anaphase transition through the stabilisation of the anaphase-promoting complex/cyclosome (APC/C) E3 ligase substrate securin (Chang et al., 2003), this transitional delay could in turn explain the lack of phospho-FAM83D and HMMR degradation. Indeed, analogous results on phospho-FAM83D and HMMR stabilisation were observed when mitotic cells were released into medium containing the APC/C inhibitor ProTAME (Zeng, Sigoillot et al., 2010) (Fig. 4D). The CK1α protein levels were unaffected by either MG132 or ProTAME treatments (Figs. 4C & D). Transcriptional analysis by qRT-PCR showed a significant two-fold increase in *FAM83D* and *HMMR* transcript levels in mitotic over asynchronous cells (Fig. 4E), suggesting that both *FAM83D* and *HMMR* are cell cycle-regulated genes, similar to *CCNB1* transcripts (Ito, 2000) (Fig. 4E). We did not detect any significant difference in CK1α transcript levels between asynchronous and mitotic cells (Fig. 4E).

The synergistic regulation of FAM83D and HMMR, and their constitutive interaction, suggested a possible role for HMMR in the regulation of FAM83D and CK1α in mitosis (Fig. 4F). Indeed, as observed in U2OS cells, a robust mitotic phospho-FAM83D mobility shift was evident in wild-type MEFs but this shift was completely absent in the *HMMR* knockout MEFs (Connell et al., 2017) (Fig. 4G). This is consistent with the notion that HMMR directs FAM83D to the spindle (Dunsch et al., 2012) and hence, in the absence of HMMR, FAM83D no longer localises to the mitotic spindle and is not phosphorylated. If this were the case, one would expect that CK1α should not be recruited to the mitotic spindle in *HMMR* knockout MEFs (Fig. 4F). After first confirming HMMR localises to the spindle in the wild-type but not *HMMR* knockout

MEFs (Fig. 4H), we observed robust CK1α mitotic spindle localisation in wild-type MEFs, but could not detect CK1α on the mitotic spindle in *HMMR* knockout MEFs (Fig. 4I). Collectively these data support the model where HMMR directs FAM83D to the spindle apparatus in mitosis, and subsequently, FAM83D recruits CK1α through the PACK1 domain. Furthermore, these findings show that the mitotic phospho-dependent mobility shift observed for FAM83D relies on the recruitment of CK1α to the mitotic spindle.

FAM83D:CK1α in FAM83D phosphorylation:

Given the absence of the FAM83D(F283A)-GFP mitotic mobility shift despite its mitotic localisation (Fig. 2D), we wondered whether targeted delivery of CK1α to FAM83D(F283A)-GFP by an anti-GFP nanobody (aGFP.16) could artificially reconstitute the FAM83D:CK1α interaction and restore the phospho-shift (Fig. 5A; Fig. EV1). Excitingly, expression of aGFP.16-CK1α in *FAM83D*$^{GFP/GFP(F283A)}$ cells rescued the phospho-mobility shift of FAM83D(F283A)-GFP, regardless of whether the cells were in mitosis or not (Fig. 5B). We also observed robust association of aGFP.16-CK1α with FAM83D(F283A)-GFP in anti-GFP IPs (Fig. 5B). The mobility shift of FAM83D(F283A)-GFP restored by the targeted delivery of CK1α relied on CK1α catalytic activity as two catalytically inactive mutants of CK1α (K46D and D136N) failed to rescue this phospho-shift completely (Fig. 5C). Critically, we observed robust co-localisation between FAM83D and CK1α on intact mitotic spindles (Fig. 5D). However, under conditions where CK1α phosphorylated FAM83G in vitro, it failed to phosphorylate recombinant FAM83D (Fig. EV5A), suggesting a cellular FAM83D context or a priming phosphorylation might be required for FAM83D phosphorylation by CK1α. Interestingly, when wild-type CK1ε, which does not interact with FAM83D nor localise to the spindle, is delivered to FAM83D(F283A)-GFP by aGFP.16, it too rescued the FAM83D phospho-shift (Fig. EV5B), suggesting the proximal catalytic activity of CK1 is sufficient for the phospho-shift and highlights the notion that subcellular localisation and substrate association are important determinants for CK1 targets. By delivering CK1α to the mitotic spindle, it is likely that FAM83D directs CK1α to phosphorylate many mitotic substrates, including itself. However, this

hypothesis relies on CK1α being functionally active when bound to FAM83D in mitosis. To test this, we employed an IP-based kinase assay strategy to isolate the FAM83D:CK1α complex, and measure phosphorylation of an optimised CK1 substrate peptide (CK1tide) using [γ-^{32}P]-ATP (Fig. 5E). Excitingly, when anti-GFP IPs from asynchronous and mitotic extracts from *FAM83D*$^{-/-}$, *FAM83D*$^{GFP/GFP}$, and *FAM83D*$^{GFP/GFP(F283A)}$ cell lines were subjected to kinase assays against CK1tide, only those from mitotic *FAM83D*$^{GFP/GFP}$ extracts, which co-precipitated endogenous CK1α, displayed significant phosphorylation of CK1tide (Fig. 5F).

FAM83D:CK1α regulates spindle positioning:

Separately, FAM83D and CK1α have been implicated in mitotic resolution and spindle/chromosome alignment (Dunsch et al., 2012, Gross, Simerly et al., 1997, Santamaria et al., 2008, Wang, Lu et al., 2013). So, we sought to test whether FAM83D and CK1α act in the same pathway in mitosis. Time lapse microscopy (Fig. 6A) showed that, compared to wild-type and *FAM83D*$^{GFP/GFP}$ knockin cells, there was a significant metaphase-to-anaphase transitional delay in the *FAM83D*$^{-/-}$ and *FAM83D*$^{GFP/GFP(F283A)}$ cell lines (Fig. 6B&C). When we analysed spindle orientation in these cells, we noted that in subconfluent *FAM83D*$^{-/-}$ and *FAM83D*$^{GFP/GFP(F283A)}$ cells, which are both deficient for spindle localisation of CK1α, spindles oriented at a fixed angle (Fig. 6D, yellow lines), which is consistent with the phenotype described following siRNA depletion of *FAM83D* (Dunsch et al., 2012). The position of the cell division axis at anaphase, relative to its expected position aligned with the long cell axis in interphase, showed significant deviation in *FAM83D*$^{-/-}$ and *FAM83D*$^{GFP/GFP(F283A)}$ cells compared to wild-type and *FAM83D*$^{GFP/GFP}$ cells (Figs. 6D, E). Excitingly, this phenotype in *FAM83D*$^{-/-}$ cells was rescued when *FAM83D cDNA* was restored at the endogenous *FAM83D* locus, with full rescue observed when restored FAM83D expression was comparable to that of wild-type cells (rescue clone 6) and a partial rescue observed when restored FAM83D expression was lower than that of wild-type cells (rescue clone 11) (Figs. 6D, E). To better study the process of spindle orientation in individual cells, we seeded individual wild-type, *FAM83D*$^{-/-}$, *FAM83D*$^{GFP/GFP}$ or *FAM83D*$^{GFP/GFP(F283A)}$ U2OS cells onto L-shaped fibronectin-coated micropatterns, which cause cells to position their spindle on a defined axis (Thery, Racine et al., 2005), and measured the

spindle orientation angles. Whereas wild-type and *FAM83D*$^{GFP/GFP}$ cells orientated their spindles along the defined, predicted axes, we observed significant deviations in the predicted spindle orientation axes with *FAM83D*$^{-/-}$ and *FAM83D*$^{GFP/GFP(F283A)}$ cells (Figs. 6F, G), with nearly 80% unable to orientate their spindles correctly (Fig. 6H) (for representative movies for each cell line, see Movie EV1-8). Again, this phenotype in the *FAM83D*$^{-/-}$ cells was fully rescued in *FAM83D* cDNA knockin rescue clone 6, and partially in clone 11 (Fig. 6H). During the process of spindle positioning analyses, we observed a random orientation of the initial spindle position (Fig. 6G), which is normally directed by the position of retraction fibres (Thery, Jimenez-Dalmaroni et al., 2007) and the assembly of subcortical actin(Fink, Carpi et al., 2011, Kwon, Bagonis et al., 2015). To monitor actin dynamics during the process of spindle assembly and orientation, cells were transfected with actin-Red Fluorescent Protein (RFP) prior to seeding on L-shaped micropatterns. In wild-type cells, we observed polarized subcortical actin adjacent to the right angle of the L-shape following DNA condensation through to anaphase (Fig. 6I). However, actin appeared to be randomly organized with respect to the micropattern in *FAM83D*$^{-/-}$ and *FAM83D*$^{GFP/GFP(F283A)}$ cells during the spindle assembly process (Fig. 6J). This observation in *FAM83D*$^{-/-}$ cells was rescued in *FAM83D* cDNA knockin clone 6, and partially in clone 11 (Fig. 6J). *FAM83D*$^{GFP/GFP}$ cells organized their actin in a manner comparable with wild-type cells (Fig. 6J). The targeted delivery of wild type (WT) or kinase-dead (KD) CK1α to FAM83D$^{GFP/GFP(F283A)}$ in knockin cells, notwithstanding the potential caveats of overexpression, allowed us to explore the role of CK1α catalytic activity in metaphase length and spindle orientation. Delivery of both WT and KD aGFP.16-CK1α resulted in shortening of the metaphase delay observed in *FAM83D*$^{GFP/GFP(F283A)}$ cells (Figs. 6A, B). However, the spindle orientation defect in *FAM83D*$^{GFP/GFP(F283A)}$ cells was rescued completely with aGFP.16-CK1α, whereas only partially with the kinase-dead aGFP.16-CK1α, in both sub-confluent cultures (Figs. 6D, E) and L-shaped micropatterns (Figs. 6G, H). Actin was correctly polarized in *FAM83D*$^{GFP/GFP(F283A)}$ cells rescued with WT, but not with the KD aGFP.16-CK1α (Fig. 6J).

We also observed frequent plasma membrane blebbing on one of the daughter cells in *FAM83D*$^{-/-}$ and *FAM83D*$^{GFP/GFP(F283A)}$ cells at the latter stages of mitosis (red arrows in Fig. 6F). This phenomenon, known as asymmetric membrane expansion (AME), is a

compensatory mechanism to ensure equal distribution of cell size following mitosis, when the spindle is misorientated (Kiyomitsu & Cheeseman, 2013). Live cell-microscopy confirmed blebbing in *FAM83D*$^{-/-}$ and *FAM83D*$^{GFP/GFP(F283A)}$ cells but not in wild-type, or *FAM83D*$^{GFP/GFP}$ cells, or in both clones rescued through knockin of *FAM83D* cDNA into the endogenous *FAM83D* locus in *FAM83D*$^{-/-}$ background (Fig. EV6A&B). Reduction of blebbing in *FAM83D*$^{GFP/GFP(F283A)}$ cells to levels seen in wild-type cells was observed when cells were rescued with WT aGFP.16-CK1α whereas an intermediate phenotype was observed with the KD aGFP.16-CK1α rescue (Fig. EV6B). Importantly, there was no difference in daughter cell size between all cell lines (Fig. EV6C). Taken together, these data indicate the FAM83D:CK1α interaction is critical for timely mitotic progression, including the processes of establishing and orienting both the mitotic spindle and the cell division axis.

Conclusion:

By conclusively placing CK1α at the mitotic spindle to ensure proper spindle orientation and timely passage through mitosis, our study adds a new paradigm to the phospho-control of mammalian cell division. Interestingly, the mechanism by which the cell cycle-regulated protein FAM83D mediates the delivery of CK1α to the mitotic spindle draws parallels with how TPX2 recruits and regulates Aurora A during mitosis. While interactors of FAM83D, including HMMR and DYNLL1, offer insights into how FAM83D localises to the mitotic spindle to recruit CK1α, the full extent of CK1α substrates that potentially mediate proper spindle positioning to ensure error-free progression through mitosis remain to be defined. Nonetheless, the findings that the FAM83D:CK1α complex acts at the mitotic spindle add to the evidence for intricate subcellular regulation of CK1 isoforms, which are implicated in many cellular processes, from Wnt signalling to the regulation of circadian rhythms, by FAM83 proteins. Given the participation of CK1 isoforms in such diverse biological processes, it is perhaps not surprising that some studies have explored and reported on roles for CK1α in the cell division cycle. Specifically, injection of CK1α antibodies into developing mouse embryos resulted in a significant delay in the progression to the first mitotic cleavage (Gross et al., 1997) and injection of CK1α morpholinos in mouse oocytes resulted in meiotic chromosomal alignment and congression defects (Wang et

al., 2013). However, these studies lacked any mechanistic understanding of how CK1α carried out these functions, as did the studies that reported somewhat-similar phenotypes resulting from siRNA knockdown of *FAM83D* in cells (Dunsch et al., 2012, Santamaria et al., 2008). Here, our findings that FAM83D binds and recruits CK1α to the mitotic spindle for proper spindle positioning illuminate mechanistic insights into the role and regulation of CK1α in mitosis, and establish that CK1α catalytic activity at the mitotic spindle is required for smooth and efficient cell division. In support of our findings, it is also interesting that observations of CK1α at the mitotic spindle have been noted by immunostaining (Brockman, Gross et al., 1992) and large-scale mitotic spindle proteomic (Sauer, Korner et al., 2005) studies. Recently, lenalidomide-induced degradation of CK1α was shown to be effective in the treatment of pre-leukemic human myelodysplastic syndrome (MDS) (Stahl & Zeidan, 2017). Similarly, genetic ablation of CK1α has been shown to activate the tumour suppressor p53, suggesting CK1α could make an anti-cancer target (Chang, Kuo et al., 2017, Chen, Li et al., 2005). Yet, other studies have demonstrated that CK1 inhibitors stabilise β-catenin and activate Wnt signalling, which promotes cell proliferation (MacDonald, Tamai et al., 2009, Schittek & Sinnberg, 2014, Teo & Kahn, 2010). Our findings would suggest that the anti-proliferative effects of CK1α inhibitors might be occurring, in part, through the inhibition of the mitotic FAM83D:CK1α pool. Often thought of as undruggable kinases due to their participation in multiple, critical processes, a method of targeting CK1 isoforms at specific locations, under certain conditions is thus warranted, yet is very challenging. However, building on data shown here, it may transpire that targeting the FAM83D:CK1α interaction may prove a viable therapeutic approach aimed at inhibition of proliferation.

Methods:

Plasmids:

Recombinant DNA procedures were performed using standard protocols as described previously(Fulcher et al., 2016). Human wild-type *FAM83D*, *CSNK1A1*, *CSNK1E*, or appropriate mutants were sub-cloned into pcDNA5/FRT/TO or pBABED P vectors (pBABED P denotes a Dundee-modified version of the pBABE Puro vector). *FAM83D*

constructs harbour a Green Fluorescence Protein (GFP) tag at the N-terminus where indicated. All constructs are available to request from the MRC-PPU reagents webpage (http://mrcppureagents.dundee.ac.uk) and the unique identifier (DU) numbers indicated above provide direct links to sequence information and cloning strategy. The following constructs were generated: pcDNA5-FRT/TO GFP-FAM83D (DU29092), pcDNA5-FRT/TO GFP-FAM83D (F283A) (DU29109), pcDNA5-FRT/TO GFP-FAM83D (D249A) (DU29110), pBABED P aGFP.16-CK1α (DU29403), pBABED P aGFP.16-CK1α (K46D) (DU29555), pBABED P aGFP.16-CK1α (D136N) (DU28707), pBABED P aGFP.16-CK1ε (DU29613) and pBABED P aGFP.16-CK1ε (D128N) (DU29629). Constructs were sequence-verified by the DNA Sequencing Service, University of Dundee (http://www.dnaseq.co.uk). For amplification of plasmids, 1 µl of the plasmid was transformed into 10 µl of *Escherichia coli* DH5α competent bacteria (Invitrogen) on ice, incubated at 42°C for 45 s, then returned to ice for 2 min, before plating on LB-agar medium plate containing 100 µg/ml ampicillin. LB plates were inverted and incubated for 16 h at 37°C. Following incubation, a single colony was picked and used to inoculate 4 ml of LB medium containing 100 µg/ml ampicillin. Cultures were grown for 18 h at 37°C in a bacterial shaker (Infors HT). Plasmid DNA was purified using a Qiagen mini-prep kit as per the manufacturer's instructions. The isolated DNA yield was subsequently analysed and quantified using a Nanodrop 1000 spectrophotometer (Thermo Scientific). For CRISPR/Cas9 gene editing, the following guide RNAs (gRNA) and Donor constructs were generated: *FAM83D* knockout: sense gRNA (DU52007), antisense gRNA (DU52023). *FAM83D* C-terminal GFP knockin: sense gRNA (DU54048), antisense gRNA (DU54054), GFP donor (DU54198). *FAM83D* C-terminal GFP knockin with F283A mutation: sense gRNA (DU57831), antisense gRNA (DU57835), GFP donor (DU57512). *FAM83D* restoration in the knockout background: sense gRNA (DU60528), antisense gRNA (DU60530), *FAM83DcDNA-IRES-GFP-polyA* donor (DU60707). *CSNK1A1* N-terminal mCherry knockin: sense gRNA (DU57522), antisense gRNA (DU57527), mCherry donor (DU57578). *CSNK1E* N-terminal mCherry knockin: sense gRNA (DU54377), antisense gRNA (DU54383), mCherry donor (DU57623). The AdPROM constructs used in this study have been described previously (Fulcher et al., 2017, Fulcher et al., 2016).

Cell Culture:

Human osteosarcoma U2OS or mouse embryonic fibroblasts (MEF) cells were grown in Dulbecco's Modified Eagles Medium (DMEM; Gibco) containing 10% (v/v) Foetal Bovine Serum (FBS; Hyclone), penicillin (100 U/ml; Lonza), streptomycin (0.1 mg/ml; Lonza) and L-glutamine (2 mM; Lonza), and cultured at 37°C, 5% CO_2 in a humidified tissue culture incubator. The wild-type and *HMMR* knockout MEFs were generated by the Maxwell laboratory, and have been described previously (Connell et al., 2017). Cells were exposed to different stimuli and compounds as described in the appropriate figure legends prior to lysis. For transient transfections, cells were transfected for 24 h with 2 µg cDNA (per 10 cm-dish) in serum free OptiMem (Gibco) with the transfection reagent polyethylenimine (PEI) as described previously (Fulcher et al., 2017, Fulcher et al., 2016, Herhaus, Al-Salihi et al., 2014). For retroviral-based infections, cells were infected with retroviruses as described previously (Fulcher et al., 2017, Fulcher et al., 2016).

Cell synchronisation:

For synchronisation, cells were arrested at prometaphase with nocodazole (100 ng/ml) for 12 h, before floating mitotic cells were isolated through mitotic shake-off. Collected mitotic cells were washed 3X in PBS before re-plating in fresh full medium for 45 mins before lysis, to allow them to progress into mitosis. Alternatively, cells were synchronised in mitosis using the Eg5 inhibitor S-trityl L-cysteine (STLC) (Skoufias et al., 2006) (5 µM) for 16 h. Following incubation, mitotic cells were isolated through shake-off, and were either washed 3X in PBS and re-plated into fresh medium, or washed 2X in ice-cold PBS, and lysed. Where appropriate, MG132 and ProTAME were used at 20 µM final concentration. For G2 arrest, cells were treated with 10 µM of the CDK1 inhibitor RO-3306 (Vassilev, 2006) for 24 h before lysis.

Live cell imaging:

U2OS cells were grown in 96-well plates (Corning) and imaged for up to 24 h at 37°C in a 5% CO_2 environmental chamber using a 40X 0.75 NA dry objective with the MetaXpress 5.0.2.0 software (Molecular Devices Inc.) on the ImageXpress Micro XL epifluorescence microscope (Molecular Devices Inc.). For the analysis of cell division kinetics, cells were stained with Hoechst (1 µg/ml) to label DNA and images were taken every 5 mins, and movies were made in the MetaXpress 5.0.2.0 software (Molecular

Devices Inc.). For actin localization, U2OS cells were seeded at 20% confluency in 24-well plates, and 1 µl CellLight Actin-RFP (Thermo Fisher Scientific) was added per 5000 cells and incubated at 37° C for 16 h. Following the incubation, U2OS cells were seeded on L-shaped micropatterns (CYTOO) at 30,000 per ml. For the analysis of actin localization, images were taken every 2 mins, and movies were made in the MetaXpress 5.0.2.0 software (Molecular Devices Inc.). Images of actin localization were projected from prophase to metaphase (Image J, z-projection standard deviation) for analysis. For the analysis of cortical membrane elongation, images were taken every 1 min, and movies were made in the MetaXpress 5.0.2.0 software (Molecular Devices Inc.).

Quantification of spindle orientation:

U2OS cells were seeded at 3,000 cells per well in 96 well plates with L-shaped micropatterns (CYTOO) at a density of 15,000 cells/ml. Prior to seeding, plates were coated with 20 µg/ml fibronectin (Sigma) for 2 h at RT. Following seeding, cells were imaged every 5 or 10 mins for up to 24 h at 37°C in a 5% CO_2 environmental chamber using an ImageXpress Micro High Content Screening System (Molecular Devices Inc.). To measure spindle orientation in subconfluent cultures, cells were seeded at 50% confluency, grown overnight and imaged as described above. Spindle angles were measured using a vector drawn through the division axis at anaphase bisecting a vector drawn through the cell's long axis determined prior to prophase.

Flow Cytometry:

For cell cycle distribution profiles, U2OS cells treated with or without synchronisation agents as described above were collected and washed 2X in PBS + 1% (v/v) FBS. Cells were fixed in 90% (v/v) ice-cold methanol for either 20 min or O/N at -20°C. Following fixation, cells were washed 2X in PBS + 1% FBS, and stained with DNA staining buffer (50 µg/ml propidium iodide, 50 µg/ml RNAse A, in PBS + 1% FBS). Following 20 min incubation at RT protected from light, samples were analysed and data acquired on a fluorescence-activated cell sorting (FACS) Canto [Becton Dickinson, (BD)] using BD FACSDIVA Software. Data was visualized using FlowJo software (Tree Star, BD). Pulse-width analysis was used to ensure the exclusion of doublets and clumps prior to evaluation of cell cycle distribution using the Watson-Pragmatic model.

Generation of *FAM83D*$^{-/-}$ knockout, *FAM83D*$^{GFP/GFP}$, *FAM83D*$^{GFP/GFP(F283A)}$, *FAM83D*$^{-/- + WT/WT}$, $^{mCherry/mCherry}$*CSNK1A1* and $^{mCherry/mCherry}$*CSNK1E* knockin cells using CRISPR/Cas9:

To generate *FAM83D*$^{-/-}$ knockout by CRISPR/Cas9 genome editing, U2OS cells were transfected with vectors encoding a pair of guide RNAs (pBABED-Puro-sgRNA1 and pX335-CAS9-D10A-sgRNA2) targeting around the first exon of *FAM83D* (1 µg each). For GFP knockins, U2OS cells were transfected with vectors encoding a pair of guide RNAs (pBABED-Puro-sgRNA1 and pX335-CAS9-D10A-sgRNA2) targeting around the stop codon of *FAM83D* (*FAM83D*$^{GFP/GFP}$) or the region surrounding the codon encoding amino acid F283 (*FAM83D*$^{GFP/GFP(F283A)}$), along with the respective donor plasmid carrying the *GFP* knockin insert and flanking homology arms (~500 bases) (3 µg each). For the *FAM83D*$^{GFP/GFP(F283A)}$ knockin, the 5' homology arm of the *GFP* donor was extended to 1000bp, in order to cover the desired site of mutation. For mCherry knockins, *FAM83D*$^{GFP/GFP}$ cells were transfected with vectors encoding a pair of guide RNAs (pBABED-Puro-sgRNA1 and pX335-CAS9-D10A-sgRNA2, 1 µg each) targeting around the start codon of *CSNK1A1 or CSNK1E,* along with the respective donor plasmid carrying the *mCherry* knockin insert and flanking homology arms (~500 bases) (3 µg each). To restore *FAM83D* in the knockout environment, we transfected the *FAM83D*$^{-/-}$ cells with a pair of guide RNAs (pBABED-Puro-sgRNA1 and pX335-CAS9-D10A-sgRNA2) targeting around the start codon of *FAM83D* which had previously been targeted for generation of *FAM83D*$^{-/-}$ knockout, along with the respective donor plasmid carrying the *FAM83DcDNA-IRES-GFP-polyA* knockin insert with flanking homology arms (~500 bases) (3 µg each). 16 h post-transfection, cells were selected in puromycin (2 µg/ml) for 48 h. The transfection process was repeated one more time. For the generation of single cell clones of knockouts, and for GFP- and mCherry-knockins, single cells were isolated by fluorescence-activated cell sorting (FACS) using an Influx cell sorter (Becton Dickinson). Single cell clones were plated on individual wells of two 96-well plates, pre-coated with 1% (w/v) gelatin to help cell adherence. Viable clones were expanded, and successful knockout or integration of *GFP*, *mCherry,* or *FAM83D* cDNA at the target locus was confirmed by both Western blotting and genomic DNA sequencing.

Generation of control and VHL-aGFP.16 AdPROM Cell Lines:

Control and VHL-aGFP.16 AdPROM cell lines were generated as described previously (Fulcher et al., 2017, Fulcher et al., 2016), using retroviral-based infections to deliver the AdPROM constructs to the *FAM83D*$^{GFP/GFP}$ U2OS cells.

Cell Lysis and Immunoprecipitation:

Cells were washed twice in ice-cold PBS, before scraping/harvesting on ice in lysis buffer (50 mM Tris-HCl pH 7.5, 0.27 M sucrose, 150 mM NaCl, 1 mM EGTA, 1 mM EDTA, 1 mM sodium orthovanadate, 10 mM sodium β-glycerophosphate, 50 mM sodium fluoride, 5 mM sodium pyrophosphate, and 1% Nonidet P40 substitute), supplemented with 1X cOmplete™ protease inhibitor cocktail (Roche). Cell extracts were either clarified and processed immediately, or snap frozen in liquid nitrogen, before storage at -80°C. Protein concentrations were determined in a 96-well format using Bradford protein assay reagent (Biorad).

For Immunoprecipitations (IPs), clarified extracts were normalised in lysis buffer to typically 1-5 mg/ml. After input aliquots were collected, lysates were incubated overnight at 4°C with protein G-sepharose beads coupled to the antibody of interest, on a rotating wheel. For anti-FLAG IPs, FLAG M2 resin (Sigma) was used; for anti-GFP IPs, GFP TRAP beads (ChromoTek) were used; and for anti-mCherry IPs, RFP (red fluorescent protein) TRAP beads (ChromoTek) were used. For anti-FAM83D IPs, anti-FAM83D-coupled sepharose beads were used, and for anti-CK1α IPs, anti-CK1α-coupled sepharose beads were used, using our in house generated anti-FAM83D and anti-CK1α antibodies respectively. Sheep IgG–coupled sepharose beads were employed as a control for endogenous IPs. Following incubation, beads were pelleted and flow-through extracts collected. Beads were washed once in lysis buffer supplemented with 250 mM NaCl, and 2-3 times in lysis buffer. For elution, beads were re-suspended in 1X SDS sample buffer, and incubated at 95°C for 5 min.

For mass-spectrometry, IPs were performed as described above except that, prior to incubation with the relevant antibody-coupled beads, extracts were pre-cleared by incubating with Protein-G sepharose beads for 1 h at 4°C on a rotating wheel. For elution, samples were boiled at 95°C for 5 min in 1X SDS sample buffer and eluted by spinning through SpinX columns (Corning).

SDS-PAGE and Western Blotting:

Reduced protein extracts (typically 10–20 μg protein) or IPs were resolved on either 8% or 13% (v/v) SDS-PAGE gels, or 4-12% NuPAGE bis-tris precast gradient gels (Invitrogen) by electrophoresis. Separated proteins were subsequently transferred onto polyvinylidene fluoride (PVDF) membranes (Millipore), before membranes were blocked in 5% (w/v) non-fat milk powder (Marvel) in TBS-T (50 mM Tris-HCl pH 7.5, 150 mM NaCl, 0.2% (v/v) Tween-20) and incubated overnight at 4°C in either 5% milk TBS-T or 5% bovine serum albumin (BSA) TBS-T with the appropriate primary antibody. Membranes were then washed 3X 10 min with TBS-T before incubating with HRP-conjugated secondary antibodies in 5% milk TBS-T for 1 h at room temperature. Membranes were then washed 3X 10 min with TBS-T before detection with enhanced chemiluminescence reagent (Millipore) and exposure to medical-grade X-ray films (Konica Minolta), as described previously (Herhaus et al., 2014, Rojas-Fernandez et al., 2015, Vogt, Dingwell et al., 2014). Alternatively, membranes were imaged using the ChemiDoc™ system (Biorad).

Antibodies:

Rabbit anti-GAPDH (cat.: 14C10, 1:5000), anti-cyclin B1 (cat.: 4138, 1:1000), anti-cyclin A2 (cat.: 4656, 1:1000), anti-CK1ε (cat.: 12448, 1:1000), anti-CK1δ (cat.: 12417, 1:1000), and anti phospho-Histone H3 (Ser 10) (cat.: 9701, 1:1000) were from Cell Signalling Technology (CST). Anti-CK1α (cat.: A301-991A, 1:1000) was from Bethyl. Anti-DYNLL1 (EP1660Y, 1:1000) was from Abcam. Anti-HMMR (cat.: ABC323, 1:1000) was from Millipore [for mouse HMMR, we used anti-CD168 (cat.: 124729, 1:1000) from Abcam]. Anti-GFP (cat.: 11814460001, 1:500) was from Roche. Anti-FAM83D (N-ter, SA102, 1:1000; C-ter, SA102, 1:1000), anti-CK1α (SA527, 3rd bleed, 1:1000), and anti-CK1ε (SA610 , 2nd bleed, 1:1000) were generated by the Division of Signal Transduction Therapy (DSTT), University of Dundee (Herhaus et al., 2014, Rojas-Fernandez et al., 2015). For mouse FAM83D, only the N-terminal FAM83D antibody recognised the target. anti-FLAG M2-Peroxidase (HRP) (cat.: A8592, 1:2000) was from Sigma. For HRP-coupled secondary antibodies, goat anti-rabbit-IgG (cat.: 7074, 1:2500) was from CST, rabbit anti-sheep-IgG (cat.: 31480,

1:5000), goat anti-rat IgG (cat.: 62-9520, 1:5000) and goat anti-mouse-IgG (cat.: 31430, 1:5000) were from Thermo Fisher.

For immunofluorescence, anti-CK1α (cat.: sc-6477, 1:100) was from Santa Cruz, and anti-CK1ε (cat.: HPA026288, 1:300) was from Sigma. The HMMR and FAM83D antibodies described above (anti-HMMR, cat.: ABC323, Milipore; anti-FAM83D, C-ter, SA102, DSTT) were also used for immunofluorescence at 1:500 dilution for human cells. For MEFs, CK1α was stained with the DSTT sheep anti-CK1α antibody (SA527, 3rd bleed, 1:500), and HMMR was stained with the murine-reactive anti-CD168 antibody (cat.: 124729, Abcam, 1:500). For signal amplification, AlexaFluor-594 donkey anti-sheep IgG (H+L) (cat.: A11058, Life Technologies, 1:300), AlexaFluor-594 goat anti-rabbit IgG (H+L) (cat.: A11012, Life Technologies, 1:500), and goat anti-mouse IgG (H+L) (cat.: A11005, Life Technologies, 1:500) were used.

Fluorescence microscopy:

Cells were seeded onto glass coverslips and treated/transfected as described above or in figure legends. Cells were washed 2X in PBS, before fixing in 4% (w/v) paraformaldehyde (PFA) for 20 min at RT. Cells were washed 2X in DMEM/10 mM HEPES, followed by incubation in DMEM/10 mM HEPES for 10 min. Cells were washed once in PBS and permeabilised for 3 min in 1.5 ml 0.2% NP40. Following permeabilisation, cells were washed 2X in PBS containing 1% (w/v) BSA, followed by incubation in PBS/BSA for 15 min. Where appropriate, coverslips were then incubated with primary antibody in PBS/BSA (typically at 1:100-1:500 dilution) at 37°C for 1-1.5 h. Cells were washed for a minimum of 3X 10 min in PBS/BSA before incubation with the secondary Alexa-Fluor conjugated antibody in PBS/BSA (1:300-500 dilution) for 60 min at RT protected from light. Coverslips were subsequently washed for 3X 10 min in PBS/BSA, and mounted on glass microscopy slides using ProLong® Gold anti-fade reagent with DAPI (Life Technologies). Coverslips were sealed with clear nail varnish and left to dry overnight before analysis on a Zeiss LSM710 confocal microscope using a 63x Plan-Apochromat objective (NA 1.40). Alternatively, cells were imaged on a Nikon TiE inverted microscope (60x objective) and visualised with NIS Elements (Nikon). Images were processed with Omero (Allan, Burel et al., 2012).

For quantification of CK1α spindle localisation, the mean pixel intensities of CK1α staining on the spindle were calculated by measuring the mean pixel intensities of CK1α in the region of interest (roi) demarcated by the outer border of the DAPI ring (hereafter referred to as the spindle roi). Subsequently, the ratio between the spindle roi and the background cytoplasmic CK1α staining was calculated, by measuring the mean cytoplasmic CK1α pixel intensities in the cytoplasmic roi, defined as the whole cell minus the spindle roi. The resulting ratios were plotted on a box plot with whiskers indicating the highest and lowest values. A ratio of >1 indicates CK1α is present on the spindle, and a ratio of ≤ 1 indicates CK1α is not present on the spindle. One might expect the theoretical ratio to be close to 1 in the *FAM83D*$^{-/-}$ cells. However, lower mean CK1α intensity in the DAPI-stained area relative to the cytoplasm implies exclusion of CK1α in DNA-rich regions. This results in a lower mean CK1α staining intensity in the overall spindle roi versus the cytoplasmic roi and therefore a ratio of less than 1. The ImageJ macro developed by Graeme Ball (Dundee Imaging Facility), used for this purpose, is included as a supplementary file.

Mass Spectrometry:

Proteins were affinity purified from clarified extracts by GFP-TRAP beads (ChromoTek) as described above. Purified proteins were resolved by 4-12% gradient SDS-PAGE, the gels were stained with InstantBlue™ (Expedeon), and gel slices covering each lane were excised and digested with trypsin. The peptides were subjected to mass spectrometric analysis performed by LC-MS-MS on a Linear ion trap-orbitrap hybrid mass spectrometer (Orbitrap-VelosPro, Thermo) coupled to a U3000 RSLC HPLC (Thermo). Peptides were trapped on a nanoViper Trap column, 2 cm x 100 µm C18 5 µm 100 Å (Thermo, 164564), then separated on a 15 cm Thermo EasySpray column (ES800) equilibrated with a flow of 300 nl/min of 3% Solvent B. [Solvent A: 2% Acetonitrile, 0.1% formic acid, 3% DMSO in H2O; Solvent B: 80% acetonitrile, 0.08% formic acid, 3% DMSO in H_2O]. The elution gradient was as follows; Time(min):Solvent B(%); 0:3, 5:3, 45:35, 47:99, 52:99, 55:3, 60:3. Data were acquired in the data-dependent mode, automatically switching between MS and MS-MS acquisition. Full scan spectra (m/z 400-1600) were acquired in the orbitrap with resolution R = 60,000 at m/z 400 (after accumulation to an FTMS Full AGC Target; 1,000,000; FTMS MSn AGC Target; 50,000). The 20 most intense ions, above a

specified minimum signal threshold (2,000), based upon a low resolution (R=15,000) preview of the survey scan, were fragmented by collision induced dissociation and recorded in the linear ion trap (Full AGC Target; 30,000. MSn AGC Target; 5,000). Data files were analysed by Proteome Discoverer 2.0 (www.ThermoScientific.com), using Mascot 2.4.1 (www.matrixscience.com), and searching the SwissProt Human database. Scaffold Q/Q+S V4.4.7 (www.ProteomeSoftware.com) was also used to examine the Mascot result files. Allowance was made for the following fixed, Carbamidomethyl (C), and variable modifications, Oxidation (M), Dioxidation (M). Error tolerances were 10ppm for MS1 and 0.6 Da for MS2. Scaffold Q/Q+S V4.4.6 (www.ProteomeSoftware.com) was used to further analyse the data and obtain values for the total unique peptide counts for each protein.

For the qualitative analysis of FAM83D interacting proteins, we employed a strict set of requirements when determining whether a protein was likely to interact with FAM83D in Asynchronous (AS), mitotic (M) or AS and M conditions. For both nocodazole and STLC treatments, only proteins which were identified by at least 5 total unique peptides were included in the analysis. Crucially, there must have been greater than 5 total unique peptides between the negative control and AS or M samples for a protein to be considered as a non-contaminant. To be deemed as an AS- or M-specific FAM83D-interacting protein, there must have been greater than 10 total unique peptides between the AS and M samples.

RNA-isolation, cDNA synthesis and qRT-PCR:

Cells were washed in PBS and RNA was isolated following the manufacture's guidelines (Qiagen). cDNA synthesis and qRT-PCR were performed as described previously (Bozatzi et al., 2018, Fulcher et al., 2017). The following primer pairs were used: FAM83D (Forward: ACGTTGATTGATGGCATCCG; Reverse: CCTTGGACTGTGGTTTTCGG), HMMR (Forward: CAAAAGAGAAACAAAGATGAG-GGG; Reverse: CCACTTGATCTGAAGCACAAC), CK1α (Forward: AATGTTAAAG-CAGAAAGCAGCAC; Reverse: TCCTCAATTCATGCTTAGAAACC), Cyclin B1 (Forward: GCAGTGC-GGGGTTTAAATCT; Reverse: GCCATGTTGATCTTCGCCTT) and GAPDH (Forward:

TGCACCACCAACTGCTTAGC; Reverse: GGCATGGACTGTGGTCATGAG). Primers were obtained from Invitrogen.

Phosphatase Assays:

Lysed extracts were subjected to GFP TRAP immunoprecipitation and washed 3X in wash buffer (200 mM NaCl, 50 mM Tris-HCl pH 7.5, 1% triton). Beads were resuspended in 20 µl phosphatase-assay buffer [New England Biolabs (cat.: PO753)] containing 1 mM $MnCl_2$, with or without λ-phosphatase (1 U) for 30 mins at 30°C, with shaking. Following incubation, beads were washed 3X in wash buffer and eluted. Input and immunoprecipitation samples were subjected to Western blotting as described above.

Purification of Recombinant Proteins:

Most recombinant proteins used in the in vitro kinase assays were purified by the Division of Signal Transduction Therapy (DSTT; University of Dundee) and the identities of the expressed proteins verified by mass spectrometry. Each protein has a unique identification number to request from the MRC-PPU Reagents website (http://mrcppureagents.dundee.ac.uk) as follows: GST-CK1α (DU329) and GST-FAM83D (DU28270). GST-FAM83G-6xHis was purified by Polyxeni Bozatzi(Bozatzi et al., 2018). Briefly, the proteins were expressed in BL21(DE3) *E. coli* as described previously (Fulcher et al., 2018), and affinity purified using GSH-sepharose or Nickel-agarose columns as appropriate.

Kinase Assays:

For peptide-based kinase assays, reactions were set up and performed as described by Hastie et al (Hastie, McLauchlan et al., 2006) except that $FAM83D^{GFP/GFP}$ immunoprecipitates, in which endogenous CK1α co-immunoprecipitated, or $^{mCherry/mCherry}$CK1α / $^{mCherry/mCherry}$CK1ε immunoprecipitates, were used instead of recombinant proteins. An optimised CK1 peptide [CK1tide, (KRRRALS*VASLPGL), where S* indicates phospho-Ser] was used as the substrate. Assays were performed using samples from 3 biological replicates.

For recombinant substrate-based kinase assays, 25 µl reactions containing 200 ng of kinase (GST-CK1α) and 2 µg of substrate (Precision protease-cleaved FAM83D, initially expressed as GST-FAM83D) in a buffer composed of 50 mM tris HCl (pH 7.5), 0.1 mM EGTA, 10 mM Magnesium acetate, 2 mM DTT, and 0.1 mM [γ^{32}P]-ATP (500 cpm/pmol). Following 30 min incubation at 30°C, assays were stopped by adding 9 µl of 4X SDS sample buffer containing 5% (v/v) β-mercaptoethanol, with subsequent heating at 95°C for 5 min. Samples were resolved by SDS-PAGE, and the gels were stained with InstantBlue (Expedeon) and dried. Radioactivity was analysed by autoradiography.

Statistical Analysis:

For qRT-PCRs, CK1α spindle localisation assays, and kinase assays, GraphPad (Prism) was used to generate plots and analyse data by unpaired Students T Test, using data from at least 3 biological replicates. A p value of <0.05 was deemed significant.

For the spindle orientation studies, GraphPad (Prism) was used to generate plots and analyze data by one way ANOVA, using data from 2 independent experiments. A p value of <0.05 was deemed significant.

Acknowledgements:

We thank GS lab members, and A. Rojas-Fernandez, M. Muqit, J. Zomerdijk, T. Ly, J. Taylor, S. Virdee, A. Saurin and A. Musacchio for their highly appreciated experimental advice and/or discussions during the course of these experiments. We thank L. Fin, J. Stark, and A. Muir for help and assistance with tissue culture, the staff at the DNA Sequencing services (School of Life Sciences, University of Dundee), and the cloning, antibody and protein production teams within the MRC PPU reagents and services (University of Dundee), coordinated by J. Hastie and H. McLauchlan. We thank the staff at the Dundee Imaging Facility (School of Life Sciences, University of Dundee), and the staff at the flow cytometry facility (School of Life Sciences, University of Dundee) for their invaluable help and advice throughout this project.

Funding:

LJF is supported by the U.K. MRC PhD studentship. The Dundee Imaging Facility is funded by the "MRC Next Generation Optical Microscopy" award [MR/K015869/1]. LJF also receives funding from the Queens College Scholarship, University of Dundee. CAM is supported by the Michael Cuccione Foundation and the Canadian Institutes of Health Research (New Investigator Salary Award and Operating Grant OBC_134038). GPS is supported by the U.K. MRC (Grant MC_UU_12016/3) and the pharmaceutical companies supporting the Division of Signal Transduction Therapy (Boehringer-Ingelheim, GlaxoSmithKline, Merck-Serono).

Author Contributions:

LJF performed most experiments, collected and analysed data, and contributed to the writing of the manuscript. ZH and LM performed experiments for spindle orientation, mitosis and blebbing assays and analysed data. TJM designed strategies and developed methods for all of the CRISPR/Cas9 gene editing, in addition to generating most of the constructs, used in the study. TJM and NTW cloned genes and performed mutagenesis experiments. ARP performed imaging experiments. AJW and RC performed flow cytometry, cell sorting, and subsequent analysis for the DNA distribution profiles. JV, RG and DGC performed mass spectrometry experiments, collected and analysed data. GB developed the ImageJ Macro for quantifying CK1α spindle localisation. CAM coordinated the spindle orientation, mitosis and blebbing assays, analysed data, and contributed to the writing of the manuscript. GPS conceived the project, analysed data and contributed to the writing of the manuscript.

Competing Interests:

The authors declare that they have no competing interests.

References:

Allan C, Burel JM, Moore J, Blackburn C, Linkert M, Loynton S, Macdonald D, Moore WJ, Neves C, Patterson A, Porter M, Tarkowska A, Loranger B, Avondo J, Lagerstedt I, Lianas L, Leo S, Hands K, Hay RT, Patwardhan A et al. (2012)

OMERO: flexible, model-driven data management for experimental biology. Nat Methods 9: 245-53
Archambault V, Glover DM (2009) Polo-like kinases: conservation and divergence in their functions and regulation. Nat Rev Mol Cell Biol 10: 265-75
Barr FA, Sillje HH, Nigg EA (2004) Polo-like kinases and the orchestration of cell division. Nat Rev Mol Cell Biol 5: 429-40
Bozatzi P, Dingwell KS, Wu KZ, Cooper F, Cummins TD, Hutchinson LD, Vogt J, Wood NT, Macartney TJ, Varghese J, Gourlay R, Campbell DG, Smith JC, Sapkota GP (2018) PAWS1 controls Wnt signalling through association with casein kinase 1alpha. EMBO Rep 19
Brockman JL, Gross SD, Sussman MR, Anderson RA (1992) Cell cycle-dependent localization of casein kinase I to mitotic spindles. Proc Natl Acad Sci U S A 89: 9454-8
Carmena M, Earnshaw WC (2003) The cellular geography of aurora kinases. Nat Rev Mol Cell Biol 4: 842-54
Chang CH, Kuo CJ, Ito T, Su YY, Jiang ST, Chiu MH, Lin YH, Nist A, Mernberger M, Stiewe T, Ito S, Wakamatsu K, Hsueh YA, Shieh SY, Snir-Alkalay I, Ben-Neriah Y (2017) CK1alpha ablation in keratinocytes induces p53-dependent, sunburn-protective skin hyperpigmentation. Proc Natl Acad Sci U S A 114: E8035-E8044
Chang DC, Xu N, Luo KQ (2003) Degradation of cyclin B is required for the onset of anaphase in Mammalian cells. J Biol Chem 278: 37865-73
Chen L, Li C, Pan Y, Chen J (2005) Regulation of p53-MDMX interaction by casein kinase 1 alpha. Mol Cell Biol 25: 6509-20
Combes G, Alharbi I, Braga LG, Elowe S (2017) Playing polo during mitosis: PLK1 takes the lead. Oncogene 36: 4819-4827
Connell M, Chen H, Jiang J, Kuan CW, Fotovati A, Chu TL, He Z, Lengyell TC, Li H, Kroll T, Li AM, Goldowitz D, Frappart L, Ploubidou A, Patel MS, Pilarski LM, Simpson EM, Lange PF, Allan DW, Maxwell CA (2017) HMMR acts in the PLK1-dependent spindle positioning pathway and supports neural development. Elife 6
Crosio C, Fimia GM, Loury R, Kimura M, Okano Y, Zhou H, Sen S, Allis CD, Sassone-Corsi P (2002) Mitotic phosphorylation of histone H3: spatio-temporal regulation by mammalian Aurora kinases. Mol Cell Biol 22: 874-85
Dunsch AK, Hammond D, Lloyd J, Schermelleh L, Gruneberg U, Barr FA (2012) Dynein light chain 1 and a spindle-associated adaptor promote dynein asymmetry and spindle orientation. J Cell Biol 198: 1039-54
Fink J, Carpi N, Betz T, Betard A, Chebah M, Azioune A, Bornens M, Sykes C, Fetler L, Cuvelier D, Piel M (2011) External forces control mitotic spindle positioning. Nat Cell Biol 13: 771-8
Fu J, Bian M, Jiang Q, Zhang C (2007) Roles of Aurora kinases in mitosis and tumorigenesis. Mol Cancer Res 5: 1-10
Fulcher LJ, Bozatzi P, Tachie-Menson T, Wu KZL, Cummins TD, Bufton JC, Pinkas DM, Dunbar K, Shrestha S, Wood NT, Weidlich S, Macartney TJ, Varghese J, Gourlay R, Campbell DG, Dingwell KS, Smith JC, Bullock AN, Sapkota GP (2018) The DUF1669 domain of FAM83 family proteins anchor casein kinase 1 isoforms. Sci Signal 11
Fulcher LJ, Hutchinson LD, Macartney TJ, Turnbull C, Sapkota GP (2017) Targeting endogenous proteins for degradation through the affinity-directed protein missile system. Open Biol 7

Fulcher LJ, Macartney T, Bozatzi P, Hornberger A, Rojas-Fernandez A, Sapkota GP (2016) An affinity-directed protein missile system for targeted proteolysis. Open Biol 6

Gross SD, Simerly C, Schatten G, Anderson RA (1997) A casein kinase I isoform is required for proper cell cycle progression in the fertilized mouse oocyte. J Cell Sci 110 (Pt 24): 3083-90

Hastie CJ, McLauchlan HJ, Cohen P (2006) Assay of protein kinases using radiolabeled ATP: a protocol. Nat Protoc 1: 968-71

Herhaus L, Al-Salihi MA, Dingwell KS, Cummins TD, Wasmus L, Vogt J, Ewan R, Bruce D, Macartney T, Weidlich S, Smith JC, Sapkota GP (2014) USP15 targets ALK3/BMPR1A for deubiquitylation to enhance bone morphogenetic protein signalling. Open Biol 4: 140065

Hochegger H, Takeda S, Hunt T (2008) Cyclin-dependent kinases and cell-cycle transitions: does one fit all? Nat Rev Mol Cell Biol 9: 910-6

Ito M (2000) Factors controlling cyclin B expression. Plant Mol Biol 43: 677-90

Kiyomitsu T, Cheeseman IM (2013) Cortical dynein and asymmetric membrane elongation coordinately position the spindle in anaphase. Cell 154: 391-402

Knippschild U, Gocht A, Wolff S, Huber N, Lohler J, Stoter M (2005) The casein kinase 1 family: participation in multiple cellular processes in eukaryotes. Cell Signal 17: 675-89

Koepp DM (2014) Cell cycle regulation by protein degradation. Methods Mol Biol 1170: 61-73

Kwon M, Bagonis M, Danuser G, Pellman D (2015) Direct Microtubule-Binding by Myosin-10 Orients Centrosomes toward Retraction Fibers and Subcortical Actin Clouds. Dev Cell 34: 323-37

Li J, Shiraki T, Igarashi K (2012) Transcription-independent role of Bach1 in mitosis through a nuclear exporter Crm1-dependent mechanism. FEBS Lett 586: 448-54

Ly T, Whigham A, Clarke R, Brenes-Murillo AJ, Estes B, Madhessian D, Lundberg E, Wadsworth P, Lamond AI (2017) Proteomic analysis of cell cycle progression in asynchronous cultures, including mitotic subphases, using PRIMMUS. Elife 6

MacDonald BT, Tamai K, He X (2009) Wnt/beta-catenin signaling: components, mechanisms, and diseases. Dev Cell 17: 9-26

Nigg EA (2001) Mitotic kinases as regulators of cell division and its checkpoints. Nat Rev Mol Cell Biol 2: 21-32

Rojas-Fernandez A, Herhaus L, Macartney T, Lachaud C, Hay RT, Sapkota GP (2015) Rapid generation of endogenously driven transcriptional reporters in cells through CRISPR/Cas9. Sci Rep 5: 9811

Santamaria A, Nagel S, Sillje HH, Nigg EA (2008) The spindle protein CHICA mediates localization of the chromokinesin Kid to the mitotic spindle. Curr Biol 18: 723-9

Sauer G, Korner R, Hanisch A, Ries A, Nigg EA, Sillje HH (2005) Proteome analysis of the human mitotic spindle. Mol Cell Proteomics 4: 35-43

Schittek B, Sinnberg T (2014) Biological functions of casein kinase 1 isoforms and putative roles in tumorigenesis. Mol Cancer 13: 231

Skoufias DA, DeBonis S, Saoudi Y, Lebeau L, Crevel I, Cross R, Wade RH, Hackney D, Kozielski F (2006) S-trityl-L-cysteine is a reversible, tight binding inhibitor of the human kinesin Eg5 that specifically blocks mitotic progression. J Biol Chem 281: 17559-69

Stahl M, Zeidan AM (2017) Lenalidomide use in myelodysplastic syndromes: Insights into the biologic mechanisms and clinical applications. Cancer 123: 1703-1713

Teo JL, Kahn M (2010) The Wnt signaling pathway in cellular proliferation and differentiation: A tale of two coactivators. Adv Drug Deliv Rev 62: 1149-55

Thery M, Jimenez-Dalmaroni A, Racine V, Bornens M, Julicher F (2007) Experimental and theoretical study of mitotic spindle orientation. Nature 447: 493-6

Thery M, Racine V, Pepin A, Piel M, Chen Y, Sibarita JB, Bornens M (2005) The extracellular matrix guides the orientation of the cell division axis. Nat Cell Biol 7: 947-53

Vassilev LT (2006) Cell cycle synchronization at the G2/M phase border by reversible inhibition of CDK1. Cell Cycle 5: 2555-6

Venerando A, Ruzzene M, Pinna LA (2014) Casein kinase: the triple meaning of a misnomer. Biochem J 460: 141-56

Vogt J, Dingwell KS, Herhaus L, Gourlay R, Macartney T, Campbell D, Smith JC, Sapkota GP (2014) Protein associated with SMAD1 (PAWS1/FAM83G) is a substrate for type I bone morphogenetic protein receptors and modulates bone morphogenetic protein signalling. Open Biol 4: 130210

Wang L, Lu A, Zhou HX, Sun R, Zhao J, Zhou CJ, Shen JP, Wu SN, Liang CG (2013) Casein kinase 1 alpha regulates chromosome congression and separation during mouse oocyte meiotic maturation and early embryo development. PLoS One 8: e63173

Zeng X, Sigoillot F, Gaur S, Choi S, Pfaff KL, Oh DC, Hathaway N, Dimova N, Cuny GD, King RW (2010) Pharmacologic inhibition of the anaphase-promoting complex induces a spindle checkpoint-dependent mitotic arrest in the absence of spindle damage. Cancer Cell 18: 382-95

Figure Legends:

Figure 1: FAM83D & CK1α interact only in mitosis:

A: Immunoblot analysis of wild type (WT), *FAM83D*$^{-/-}$ knockout (KO) and *FAM83D*$^{GFP/GFP}$ knockin (KI) U2OS cell lines. **B:** Proteomic analysis on asynchronous (AS), Nocodazole- or STLC-synchronised mitotic (M) *FAM83D*$^{GFP/GFP}$ knockin (KI) U2OS KI cells. The Venn diagram depicts the top proteins which were identified as FAM83D interactors in AS, M, or both AS and M conditions, in both nocodazole and STLC treatments (for a detailed analysis procedure, see the methods section). **C:** Schematic highlighting whether a mitotic interaction was previously known between FAM83D and the interacting proteins identified in B. **D:** AS or nocodazole-synchronised M KI cells were lysed and subjected to GFP-TRAP immunoprecipitations (IP). Extracts (input) and IP samples were analysed by immunoblotting (IB) with the

indicated antibodies. **E:** KI cells synchronised in mitosis with either nocodazole (M Noc.) or STLC (M STLC) were collected by shake-off, and drug-treated cells that remained adherent after shake-off (AS Noc.; AS STLC) were lysed and subjected to GFP-TRAP IP. AS cells and free-GFP-expressing 2G-*PAI1* U2OS cells were included as controls. Input and IP samples were analysed by IB with the indicated antibodies. **F:** Propidium iodide staining analyses revealing cell cycle distribution profiles for the samples described in E. **G:** AS or nocodazole-synchronised (M) WT U2OS cells were subjected to IP with either IgG- or anti-FAM83D-coupled sepharose beads. Input and IP samples were analysed by IB with the indicated antibodies. **H:** As in G. except that anti-CK1α-coupled sepharose beads was used. **I:** KI cells were synchronised in G2 with RO-3306, or arrested in mitosis (M) using STLC. STLC-treated shake-off cells were washed and re-plated, and cells lysed at the indicated time points after STLC wash-out. Cell lysates were subjected to GFP-TRAP IP and input and IP extracts analysed by IB with the indicated antibodies. **H:** As in F, except for H. All blots are representative of at least 3 independent experiments.

Figure 2: FAM83D recruits CK1α to the spindle:

A: STLC-synchronised mitotic (M) Wild type (WT), *FAM83D*$^{-/-}$ knockout (KO) and *FAM83D*$^{GFP/GFP}$ knockin (KI) U2OS cells were subjected to anti-CK1α immunofluorescence and GFP fluorescence microscopy. DNA is stained with DAPI. Scale bars, 20 μM. **B:** As in A. except that KO, KI, and *FAM83D*$^{GFP/GFP(F283A)}$ knockin (FA) U2OS cells were used. Scale bars, 20 μM. **C:** Quantification of CK1α spindle localisation for the cells described in panels A. and B. Cell images denote the measured regions used to calculate the ratios on the box plot. Box plot whiskers denote the minimum and maximum measured values. *** , $P<0.0001$. Analysis was performed on the indicated number of cells, from 2 independent experiments. **D:** The cell lines described in B. were STLC-synchronised and mitotic cells (M) isolated by shake off. Asynchronous (AS) cells were included as a control. Cells were lysed and subjected to GFP-TRAP immunoprecipitation (IP) and subsequent immunoblotting (IB) with the indicated antibodies. **E:** Schematic illustration of the AdPROM-mediated degradation of FAM83D. VHL; Von Hippel Lindau protein, CUL2; Cullin 2, RBX1; RING-box protein 1, E2; E2 ubiquitin-conjugating enzyme, aGFP.16; anti-GFP.16 nanobody. **F:** KI cells were infected with retroviruses encoding either VHL, aGFP.16, or VHL-

aGFP.16. Uninfected cells were used as a control. Cells were lysed and subjected to IB with the indicated antibodies. **G:** The cell lines described in F. were subjected to anti-CK1α immunofluorescence and GFP fluorescence microscopy. DNA is stained with DAPI. Scale bars, 20 μM. All blots are representative of at least 3 independent experiments.

Figure 3: FAM83D and CK1α in unperturbed cells:

A: Schematic illustrating the CRISPR-mediated strategy used to reintroduce FAM83D into a *FAM83D* knockout background. **B:** *FAM83D*$^{-/-}$ (KO), wild-type (WT), and two independent clones from a CRISPR/Cas9-mediated knockin rescue of *FAM83D* in *FAM83D*$^{-/-}$ cells (c. 6 and c. 11) were synchronized in mitosis (M) with STLC. AS cells were included as a control. Cells were lysed and subjected to immunoblotting (IB) with the indicated antibodies. **C-D:** The cell lines described in B. were STLC-synchronized in mitosis, fixed, and stained with antibodies recognizing FAM83D (C) or CK1α (D). Representative images of mitotic cells are included. Scale bars, 20 μM. **E:** Quantification of CK1α spindle localization for the experiment described in D. using the same strategy employed in Fig. 2C. ***, P<0.0001. Analysis was performed on the indicated number of cells, from 1 independent experiment. **F:** The cell lines described in B. were STLC-synchronized in mitosis (M) or left AS, lysed and subjected to immunoprecipitation (IP) with anti-FAM83D-coupled sepharose beads, before IB with the indicated antibodies. **G:** Asynchronous (AS) *FAM83D*$^{GFP/GFP}$/$^{mCherry/mCherry}$*CSNK1A1* knockin U2OS cells were fixed and imaged. Representative images from the indicated cell cycle stages are included. Scale bars; 10 μM. All blots are representative of at least 3 independent experiments.

Figure 4: FAM83D regulation during cell cycle:

A: Nocodazole-synchronised mitotic *FAM83D*$^{GFP/GFP}$ knockin (KI) U2OS cells were lysed and subjected to GFP-TRAP immunoprecipitation (IP), followed by incubation ± λ-phosphatase. Asynchronous (AS) cells were used as a control. Whole cell extracts (input) and IP samples were subjected to immunoblotting (IB) with the indicated antibodies. **B:** STLC-synchronised mitotic wild-type U2OS cells were lysed at the indicated time points following STLC washout. AS cells were used as a control. Lysed extracts were subjected to IB with the indicated antibodies. **C:** As in B. except that cells

were released into medium ± MG132. **D:** As in C. except that ProTAME was used instead of MG132. **E:** STLC-synchronised mitotic wild-type U2OS cells were subjected to qRT-PCR analysis using primers for *FAM83D*, *HMMR*, *CSNK1A1,* and *CCNB1*. AS cells were used as a control. Error bars, SEM; *, P<0.01. **F:** schematic representing the predicted effects of *HMMR* knockout on FAM83D:CK1α delivery to the mitotic spindle. In the absence of HMMR, no FAM83D and by extension no CK1α can localise to the spindle. **G:** STLC-synchronised mitotic wild-type (WT) and *HMMR* knockout (KO) mouse embryonic fibroblasts (MEFs) were lysed and subjected to IB with the indicated antibodies. AS cells were included as a control. **H-I:** The cells described in G. were STLC-synchronised in mitosis and subjected to immunofluorescence microscopy with an anti-HMMR antibody (H) or an anti-CK1α antibody (I). DNA is stained with DAPI. Scale bars, 20 μM. All blots are representative of at least 3 independent experiments.

Figure 5: FAM83D:CK1α in FAM83D phosphorylation:

A: Schematic representation of the anti-GFP nanobody (aGFP.16) based targeting strategy used to deliver CK1α to the CK1-binding-deficient FAM83D(F283A)-GFP mutant. **B:** STLC-synchronised mitotic $FAM83D^{GFP/GFP}$ knockin (KI), $FAM83D^{GFP/GFP(F283A)}$ (FA) and $FAM83D^{GFP/GFP(F283A)}$ stably expressing aGFP.16-CK1α (FA + aGFP.16-CK1α) cells were subjected to GFP-TRAP immunoprecipitation (IP), followed by immunoblotting (IB) with the indicated antibodies. Asynchronous (AS) cells were used as controls. **C:** FA cells were infected with retroviruses encoding wild-type aGFP.16-CK1α (WT), or aGFP.16-CK1α with one of two distinct CK1α kinase-inactive mutations (D136N or K46D). Uninfected cells (-) were included as a control. Cells were lysed, subjected to anti-GFP IP and IB with the indicated antibodies. **D:** Immunofluorescence analysis for the cells described in B. following synchronisation with STLC. Cells were stained using anti-CK1α antibody, and DNA is stained with DAPI. Scale bars, 20 μM. **E:** Schematic depicting the IP kinase assay strategy used to test whether FAM83D-bound CK1α was catalytically active. **F:** $FAM83D^{-/-}$ knockout (KO), KI, and FA cells were synchronised in mitosis (M) using STLC. Lysed extracts were subjected to anti-GFP IPs, followed by ATP [γ-32P] kinase assays, using an optimised CK1 substrate peptide (CK1tide). AS cells were used as controls. Assays include 3 biological replicates. Error bars, SEM. Input and IP samples were analysed

by IB with the indicated antibodies. All blots are representative of at least 3 independent experiments.

Figure 6: FAM83D:CK1α regulates spindle positioning: **A.** Representative images initiating at metaphase for mitotic U2OS cell lines stained with Hoechst, taken every 5 mins as they progress through division. Mitotic stage was determined by chromosome condensation and is indicated by the coloured boxes. Scale bar, 20 μm. **B**. Graphical representation for the kinetics of transition from metaphase alignment (yellow) to anaphase (green), and cytokinesis (blue). 100 mitotic cells per genotype are plotted; n=2. **C**. Length of time needed to transition from metaphase to anaphase. Mean of 100 mitotic cells per genotype are plotted; n=2. Error bars, SEM. ***, $p< 0.0001$. **D**. Representative bright field images for mitotic U2OS cells indicating the long axis during interphase (white line) preceding mitosis, and the division axis determined at anaphase (yellow line). Scale bar, 20 μm. **E**. Percentage of oriented divisions for U2OS cells grown in subconfluent cultures. An oriented division axis was defined as being less than 30° removed from the long axis of the interphase cell. Mean of 50 cells per genotype are plotted, n=2. Error bars, SEM. ***, $p< 0.0001$. **F.** Representative images of mitotic U2OS cells stained with Hoechst and grown on L-shaped micropatterns previously coated with fibronectin. The position of metaphase chromosomes, which is plotted in panel H, is indicated (yellow line) as is the presence of cortical blebbing (red arrows). Scale bar, 20 μm. **G.** Circular graphs, superimposed on L-shaped micropattern, show the distribution of cell division angles measured at anaphase. Angles for 100 U2OS cells are plotted per genotype, n=2. Metaphase position is indicated (yellow line) and the percentages of division angles ± 15° from the expected axis (red line) are indicated. **H**. Percentage of metaphase U2OS cells that align chromosomes outside of the expected axis (angles ± 15°). Mean of 100 cells per genotype are plotted, n=2. Error bars, SEM. ***, $p< 0.0001$. **I.** Representative images of RFP-actin localization in mitotic U2OS cells grown on fibronectin-coated, L-shaped micropatterns, which is superimposed. Arrowheads indicate polarized cortical actin. Heatmap shows the intensity of RFP-actin localization (Image J z-projection standard deviation) as the cell progresses from prophase to metaphase (12- 24 mins). Scale bar, 20 μm. **J.** Heatmap additive intensities of RFP-actin localization in two representative

mitotic U2OS cells for each genotype grown on fibronectin-coated, L-shaped micropatterns. Arrowheads indicate polarized cortical actin.

Figure EV1: Schematic of the CRISPR/Cas9 gene editing strategies, and retrovirally-expressed nanobody-based systems used in this study:

Schematic detailing the CRISPR/Cas9 gene editing strategies employed to generate the indicated cell lines (left-hand side). The schematic on the right-hand side details the retrovirally-expressed nanobody-based degradation (VHL-aGFP.16), and targeting (aGFP.16-CK1) strategies used in this study.

Figure EV2: FAM83D is not responsible for recruiting CK1ε or HMMR to the spindle in mitosis:

A: Wild type (WT), *FAM83D*$^{-/-}$ knockout (KO) and *FAM83D*$^{GFP/GFP}$ knockin (KI) U2OS cells were synchronised in mitosis with STLC, before being subjected to anti-CK1ε immunofluorescence and GFP fluorescence microscopy. DNA is stained with DAPI. **B:** As in A. except that cells were subjected to anti-HMMR immunofluorescence microscopy. Scale bars, 20 μM.

Figure EV3: Testing CK1-binding-deficient FAM83D mutants in mitosis:

A: *FAM83D* KO U2OS cells were transiently transfected with vectors encoding GFP-FAM83D (WT), GFP-FAM83D (F283A) (FA), or GFP-FAM83D (D249A) (DA). Untransfected cells were included as a control (-). Following transfection, cells were synchronised in mitosis with STLC. Mitotic cells were collected, lysed and subjected to anti-GFP immunoprecipitation (IP) with GFP TRAP beads. Whole cell extracts (input) and IP samples were immunoblotted (IB) with the indicated antibodies. **B:** *FAM8D*$^{GFP/GFP(F283A)}$ knockin U2OS cells (clone 19) were synchronised in mitosis with STLC (M). Asynchronous (AS) cells were included as a control. Cells were lysed and subjected to anti-GFP immunoprecipitation with GFP TRAP beads. Whole cell extracts (input) and IP samples were immunoblotted (IB) with the indicated antibodies. **C:** The cell line described in B. were subjected to anti- CK1α immunofluorescence and GFP fluorescence microscopy. DNA is stained with DAPI. Scale bars, 20 μM.

Figure EV4: Verification of $^{mCherry/mCherry}$*CSNK1A1* and $^{mCherry/mCherry}$*CSNK1E* U2OS knockin cells:

A: Wild-type (WT), *FAM83D*$^{GFP/GFP}$ knockin, *FAM83D*$^{GFP/GFP}$ knockin with $^{mCherry/mCherry}$*CSNK1A1* clone 4, and *FAM83D*$^{GFP/GFP}$ knockin with $^{mCherry/mCherry}$*CSNK1E* clone 5 U2OS cells were lysed, and subjected to immunoblotting (IB) with the indicated antibodies. **B:** The cell lines described in A. were synchronized in mitosis with STLC (M) or left asynchronous (AS). Cells were lysed and subjected to immunoprecipitation (IP) with RFP-TRAP beads, before immunoblotting (IB) with the indicated antibodies. **C:** *FAM83D*$^{GFP/GFP}$ knockin, *FAM83D*$^{GFP/GFP}$ knockin with $^{mCherry/mCherry}$*CSNK1A1* clone 4, and *FAM83D*$^{GFP/GFP}$ knockin with $^{mCherry/mCherry}$*CSNK1E* clone 5 U2OS cells were lysed and subjected to immunoprecipitation (IP) with RFP-TRAP beads, and subjected to an in vitro [$^{\gamma 32}$P]-ATP kinase assay using an optimized CK1 substrate peptide (CK1tide) and radiolabeled ATP. n=3, Error bars, SEM, ***, P<0.0001. **D:** Asynchronous *FAM83D*$^{GFP/GFP}$ / $^{mCherry/mCherry}$*CSNK1E* knockin U2OS cells were fixed and imaged. Representative images from the indicated cell cycle stages are included. Scale bar; 10 μM.

Figure EV5: CK1α does not appear to phosphorylate FAM83D *in vitro*:

A: An *in vitro* kinase assay was set up using recombinant GST-FAM83D, and GST-CK1α. GST-FAM83D without CK1α is a negative control. Recombinant GST-FAM83G-6xHis serves as a positive control for CK1α activity. Following incubation with radioactive ATP, reactions were stopped and subjected to SDS-PAGE. The gel was stained with Instant Blue and imaged, before subjection to autoradiography (autorad). **B:** *FAM83D*$^{GFP/GFP(F283A)}$ cells were infected with retroviruses encoding wild-type aGFP.16-CK1ε (WT), or a kinase-dead aGFP.16-CK1ε (D128N) mutant (KD). Uninfected cells (-) were included as a control. Cells were lysed, subjected to anti-GFP immunoprecipitations (IP) and immunoblotted (IB) with the indicated antibodies.

Figure EV6: Disruption of the FAM83D:CK1α interaction promotes symmetric membrane elongation but does not affect daughter cell size.

A: Representative bright field images initiating at metaphase for mitotic U2OS cells

taken every 1 min as they progress through division. Asymmetric membrane elongation, or membrane blebbing, is indicated by red arrowheads and only occurred on one daughter cell. Scale bar = 20 μm. **B**: Percentage of mitotic cells that displayed membrane blebbing. Mean of 50 cells per genotype are plotted from 2 independent experiments. Error bars denote SEM. ** $p < 0.005$, ANOVA. **C**: Daughter cell size ratio following U2OS cell division remains unchanged. Mean of 50 cells per genotype are plotted from 2 independent experiments. Error bars denote SEM.

Movie EV1: Wild-type U2OS cell divides along the hypotenuse of an L-shaped, fibronectin-coated micropattern. A representative wild-type U2OS cell was imaged for 90 mins with images captured at 10-min intervals. Cell division is shown through time at 1 frame per second with the nucleus counterstained with Hoechst (shown in red), and the L-shape micropattern and expected position of metaphase chromosomes overlaid in white dashed lines. The actual position of metaphase chromosomes is shown with a red line in the two frames prior to anaphase. Scale bar = 20 μm.

Movie EV2: *FAM83D*$^{-/-}$ U2OS cell fails to divide along the hypotenuse of an L-shaped, fibronectin-coated micropattern. A representative *FAM83D*$^{-/-}$ U2OS cell was imaged for 100 mins with images captured at 10-min intervals. Cell division is shown through time at 1 frame per second with the nucleus counterstained with Hoechst (shown in red), and the L-shape micropattern and expected position of metaphase chromosomes overlaid in white dashed lines. The actual position of metaphase chromosomes is shown with a red line in the two frames prior to anaphase. Scale bar = 20 μm.

Movie EV3: *FAM83D*$^{GFP/GFP}$ U2OS cell divides along the hypotenuse of an L-shaped, fibronectin-coated micropattern. A representative *FAM83D*$^{GFP/GFP}$ U2OS cell was imaged for 70 mins with images captured at 10-min intervals. Cell division is shown through time at 1 frame per second with the nucleus counterstained with Hoechst (shown in red), and the L-shape micropattern and expected position of metaphase chromosomes overlaid in white dashed lines. The actual position of metaphase chromosomes is shown with a red line in the two frames prior to anaphase. Scale bar = 20 μm.

Movie EV4: *FAM83D*$^{GFP/GFP(F283A)}$ U2OS cell fails to divide along the hypotenuse of an L-shaped, fibronectin-coated micropattern. A representative *FAM83D*$^{GFP/GFP(F283A)}$ U2OS cell was imaged for 150 mins with images captured at 10-min intervals. Cell division is shown through time at 1 frame per second with the nucleus counterstained with Hoechst (shown in red), and the L-shape micropattern and expected position of metaphase chromosomes overlaid in white dashed lines. The actual position of metaphase chromosomes is shown with a red line in the two frames prior to anaphase. Scale bar = 20 μm.

Movie EV5: *FAM83D*$^{GFP/GFP(F283A)}$+aGFP.16-CK1α cell divides along the hypotenuse of an L-shaped, fibronectin-coated micropattern. A representative *FAM83D*$^{GFP/GFP(F283A)}$ +aGFP.16-CK1α U2OS cell was imaged for 110 mins with images captured at 10-min intervals. Cell division is shown through time at 1 frame per second with the nucleus counterstained with Hoechst (shown in red), and the L-shape micropattern and expected position of metaphase chromosomes overlaid in white dashed lines. The actual position of metaphase chromosomes is shown with a red line in the two frames prior to anaphase. Scale bar = 20 μm.

Movie EV6: *FAM83D*$^{GFP/GFP(F283A)}$+aGFP.16-CK1α(K46D) cell fails to divide along the hypotenuse of an L-shaped, fibronectin-coated micropattern. A representative *FAM83D*$^{GFP/GFP(F283A)}$ +aGFP.16-CK1α(K46D) U2OS cell was imaged for 90 mins with images captured at 10-min intervals. Cell division is shown through time at 1 frame per second with the nucleus counterstained with Hoechst (shown in red), and the L-shape micropattern and expected position of metaphase chromosomes overlaid in white dashed lines. The actual position of metaphase chromosomes is shown with a red line in the two frames prior to anaphase. Scale bar = 20 μm.

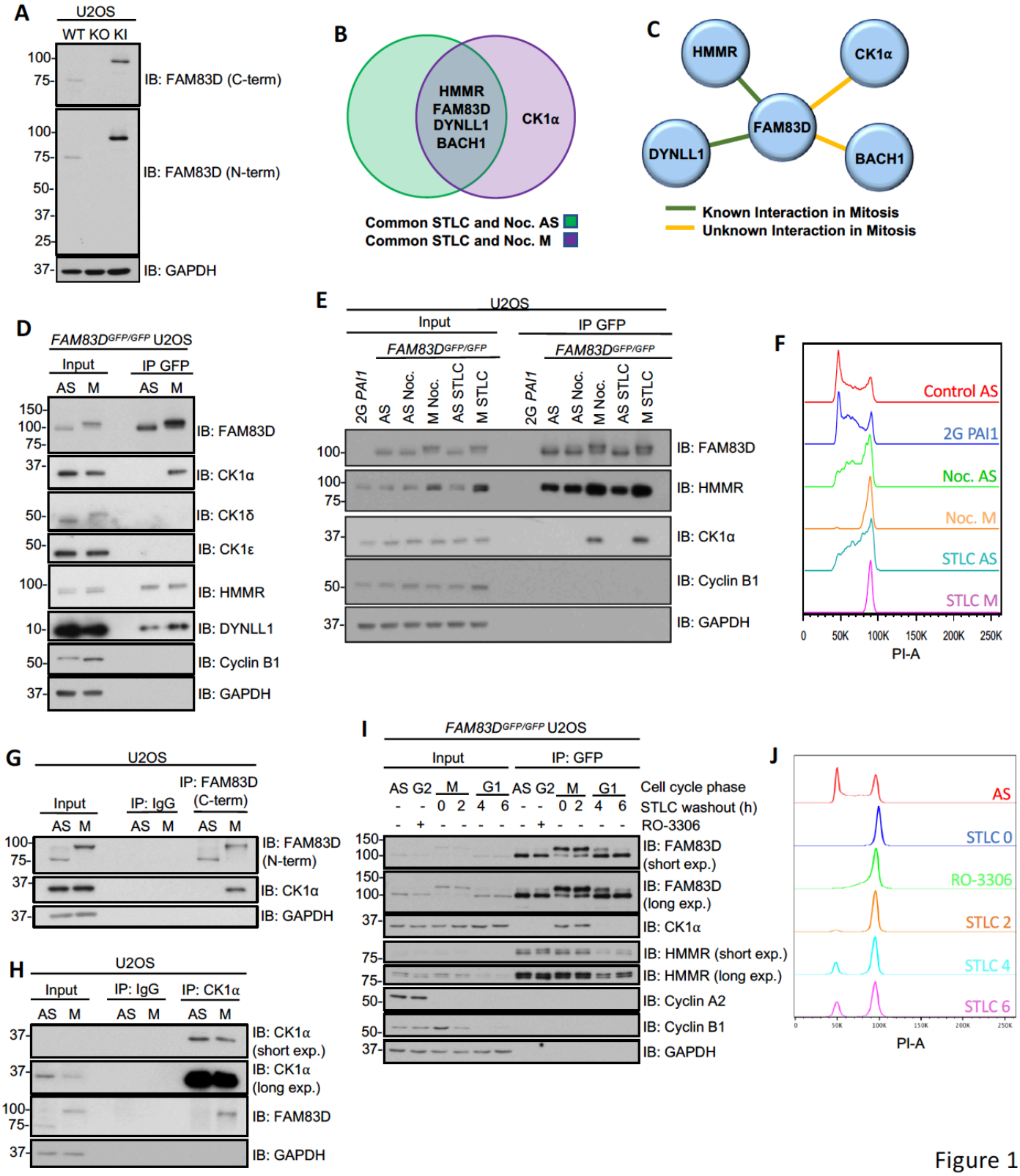

Figure 1

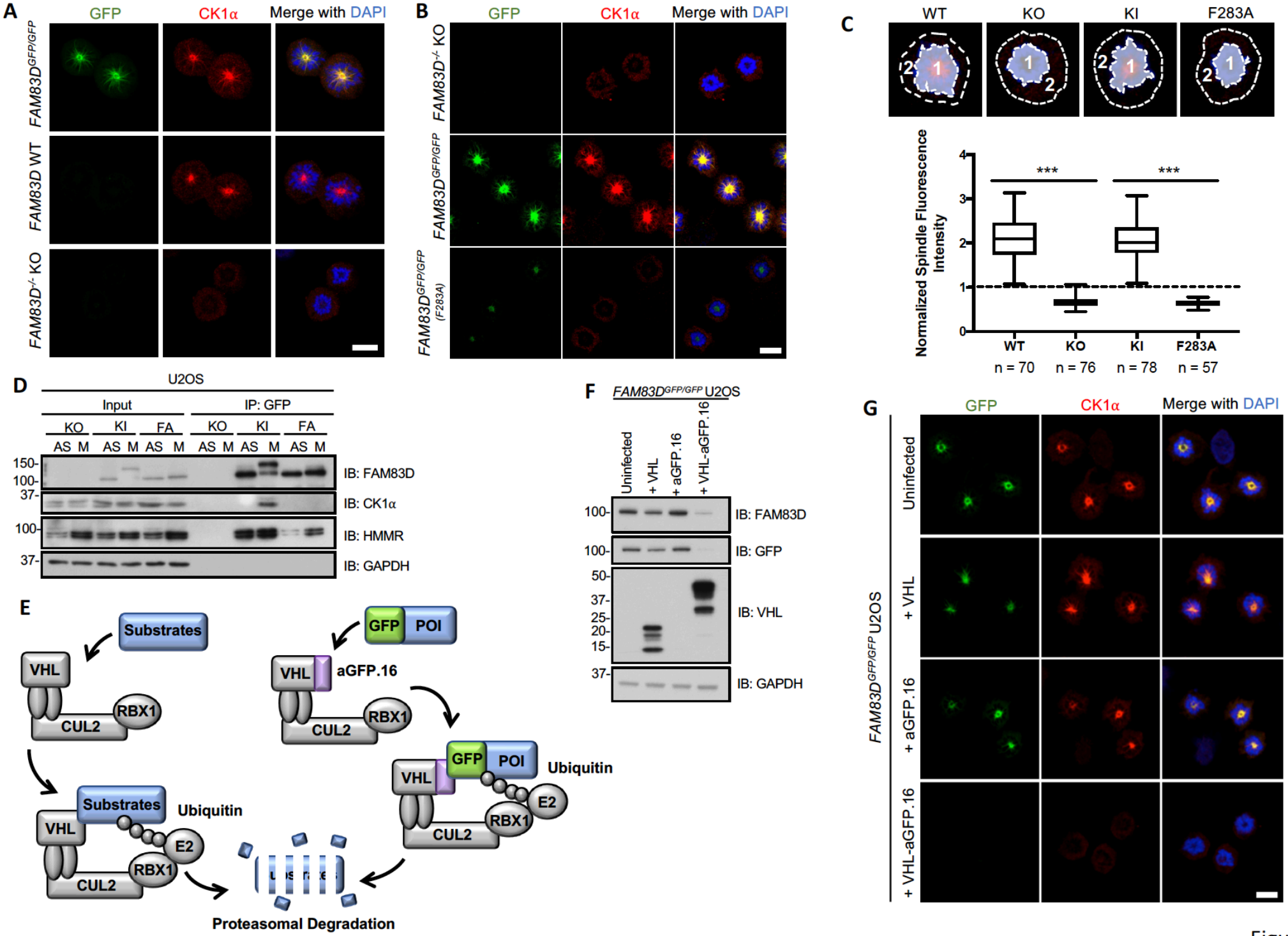
A
GFP
CK1α
Merge with DAPI
FAM83D GFP/GFP
FAM83D WT
FAM83D -/- KO
B
GFP
CK1α
Merge with DAPI
FAM83D -/- KO
FAM83D GFP/GFP
FAM83D GFP/GFP (F283A)
C
WT
KO
KI
F283A
Normalized Spindle Fluorescence Intensity
***
***
WT
KO
KI
F283A
n = 70
n = 76
n = 78
n = 57
D
U2OS
Input
IP: GFP
KO
KI
FA
AS M
150-
100-
37-
IB: FAM83D
IB: CK1α
IB: HMMR
IB: GAPDH
E
Substrates
VHL
CUL2
RBX1
GFP
POI
aGFP.16
Ubiquitin
E2
Proteasomal Degradation
F
FAM83D GFP/GFP U2OS
Uninfected
+ VHL
+ aGFP.16
+ VHL-aGFP.16
100-
50-
37-
25-
20-
15-
IB: FAM83D
IB: GFP
IB: VHL
IB: GAPDH
G
GFP
CK1α
Merge with DAPI
FAM83D GFP/GFP U2OS
Uninfected
+ VHL
+ aGFP.16
+ VHL-aGFP.16

Figure 2

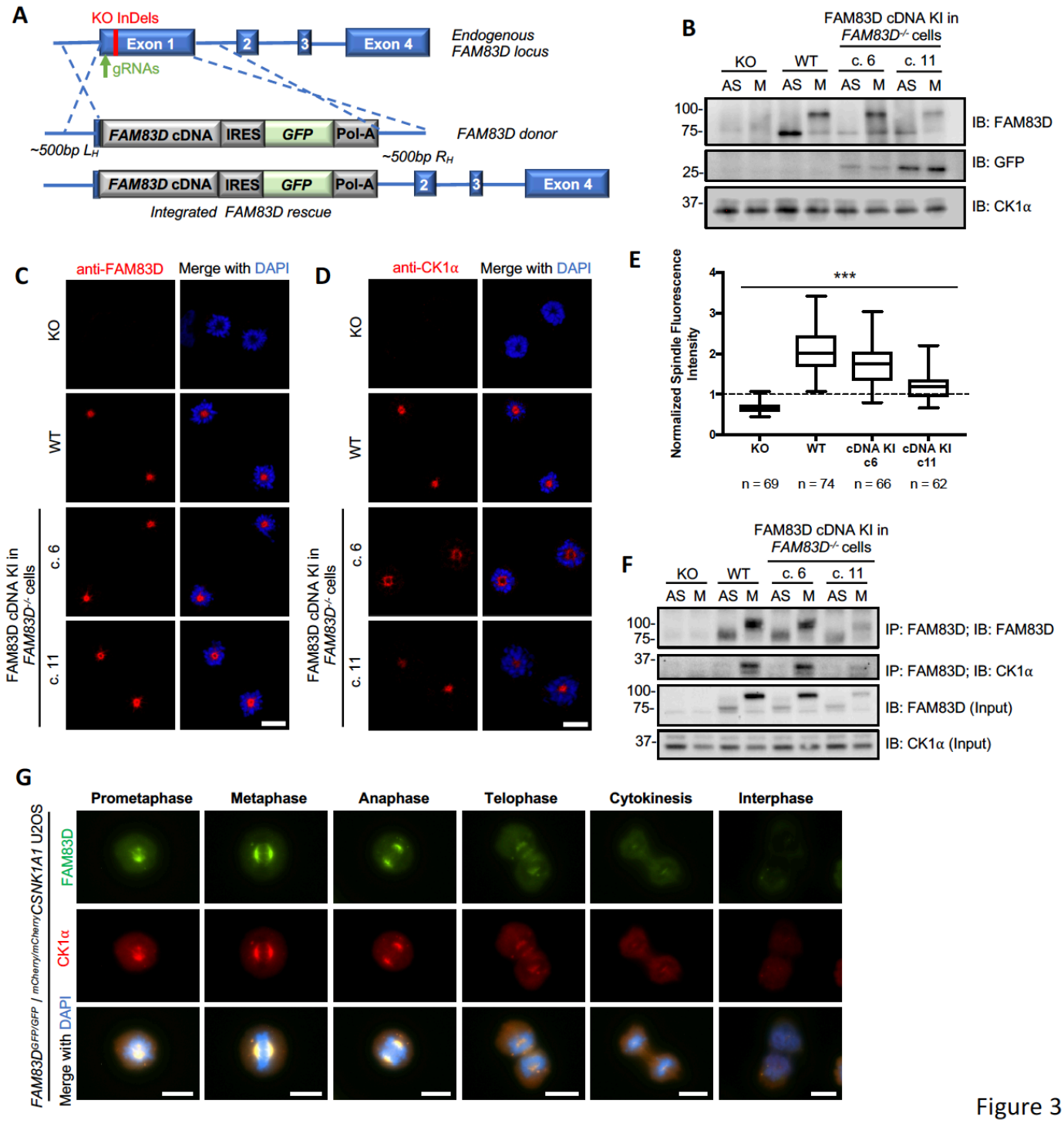

Figure 3

Figure 4

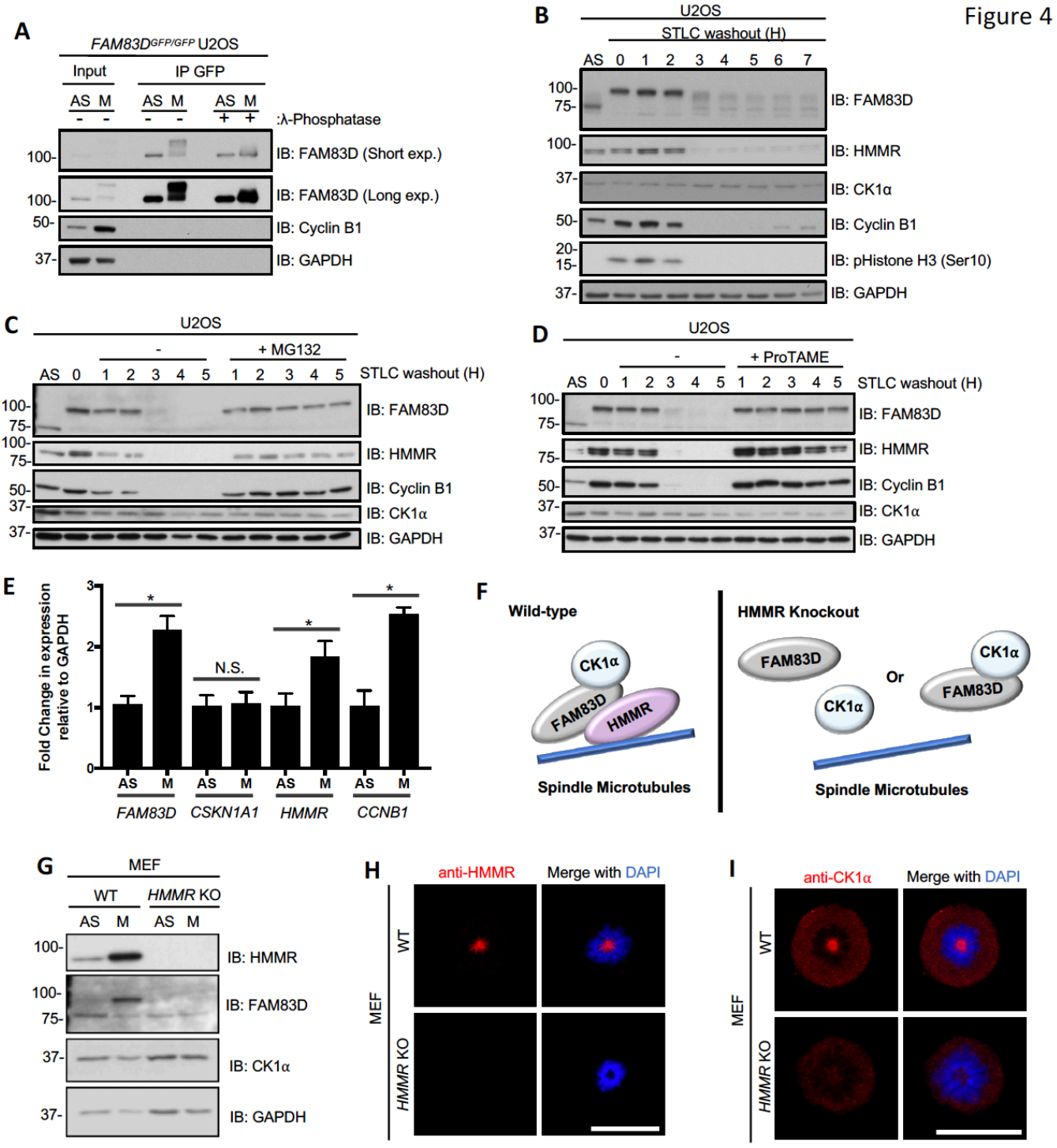

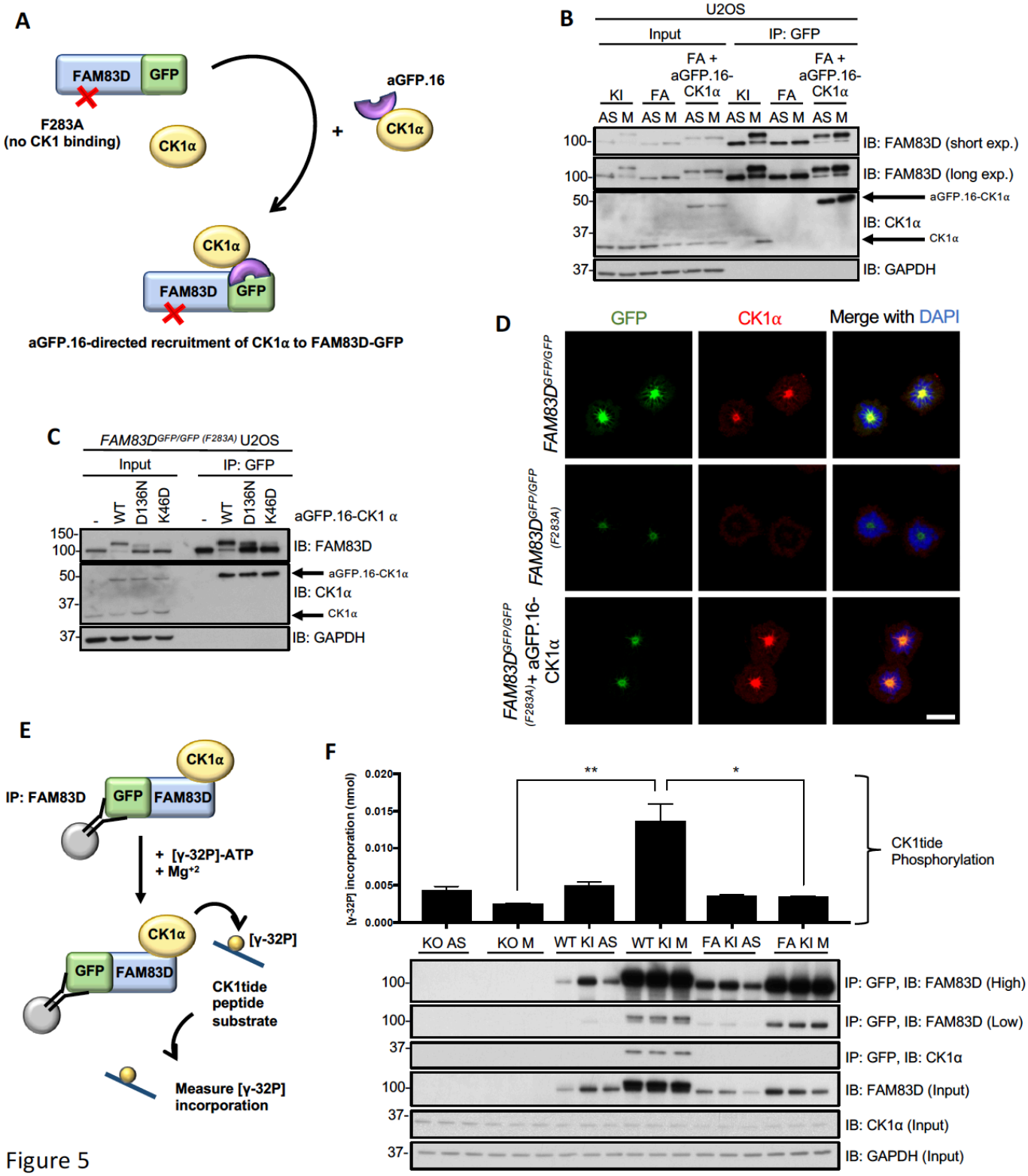

Figure 5

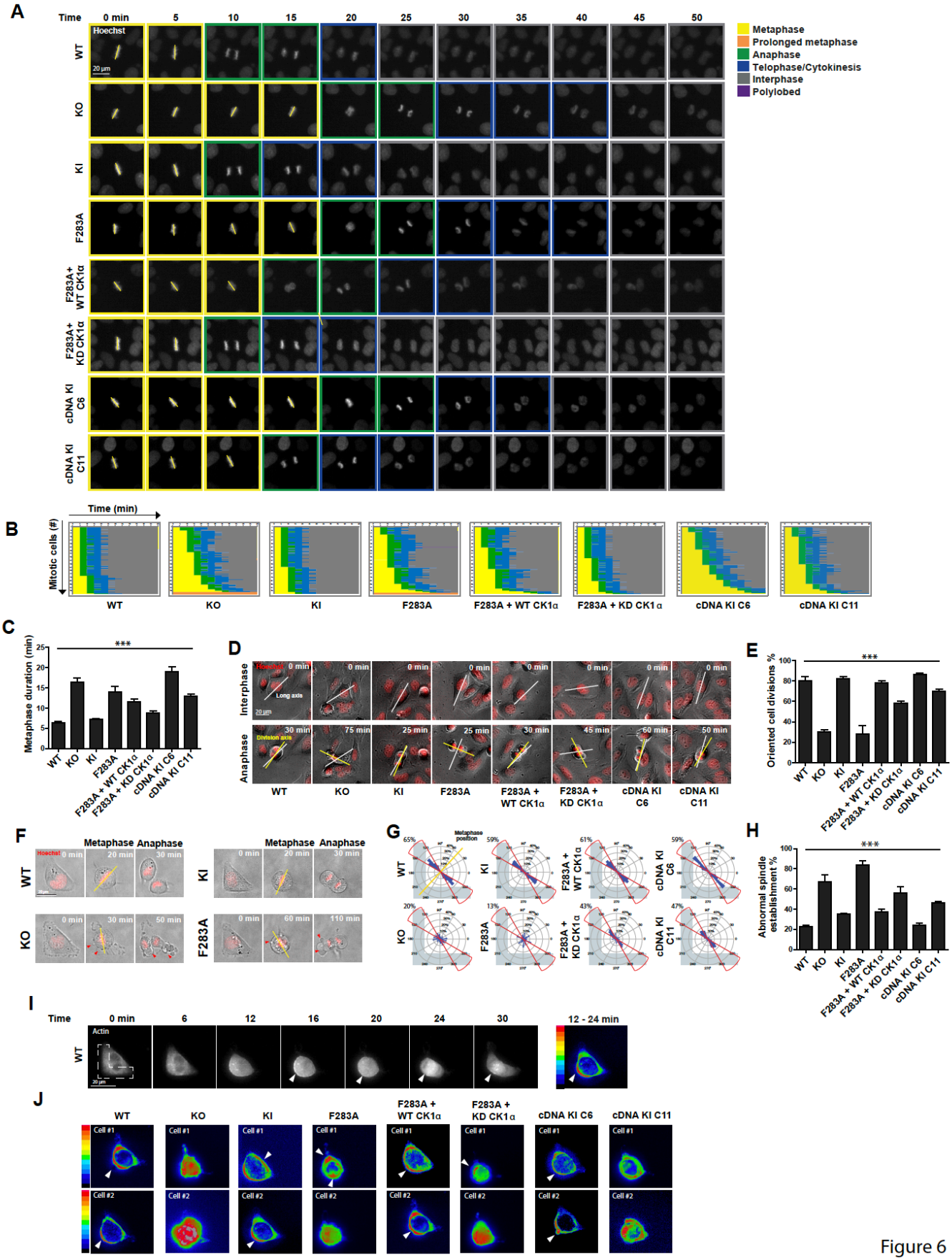

Figure 6

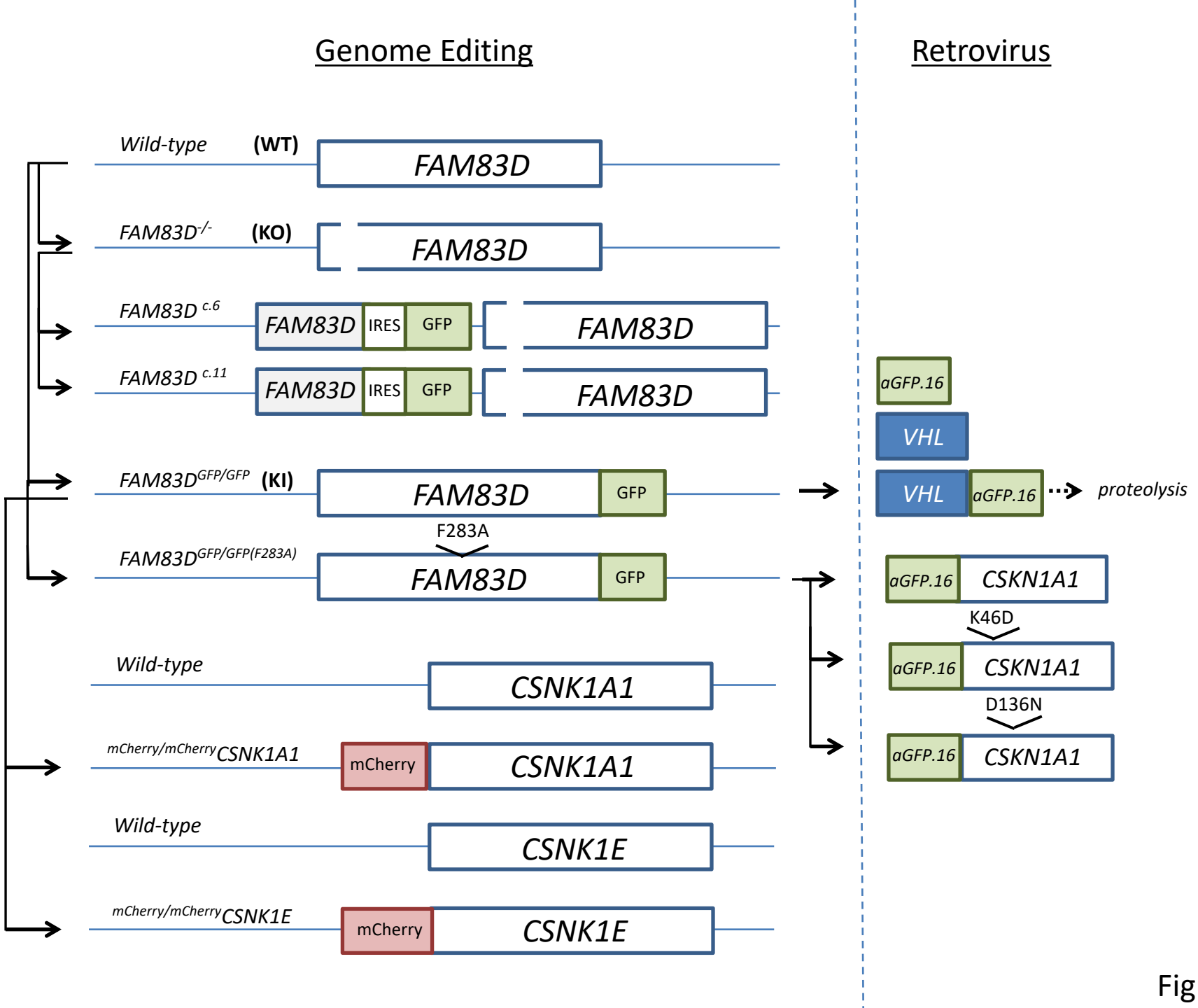
Genome Editing
Retrovirus
Wild-type (WT)
FAM83D
FAM83D-/- (KO)
FAM83D
FAM83D c.6
FAM83D
IRES
GFP
FAM83D
FAM83D c.11
FAM83D
IRES
GFP
FAM83D
aGFP.16
VHL
FAM83DGFP/GFP (KI)
FAM83D
GFP
VHL
aGFP.16
proteolysis
F283A
FAM83DGFP/GFP(F283A)
FAM83D
GFP
aGFP.16
CSKN1A1
K46D
aGFP.16
CSKN1A1
D136N
aGFP.16
CSKN1A1
Wild-type
CSNK1A1
mCherry/mCherryCSNK1A1
mCherry
CSNK1A1
Wild-type
CSNK1E
mCherry/mCherryCSNK1E
mCherry
CSNK1E

Figure EV1

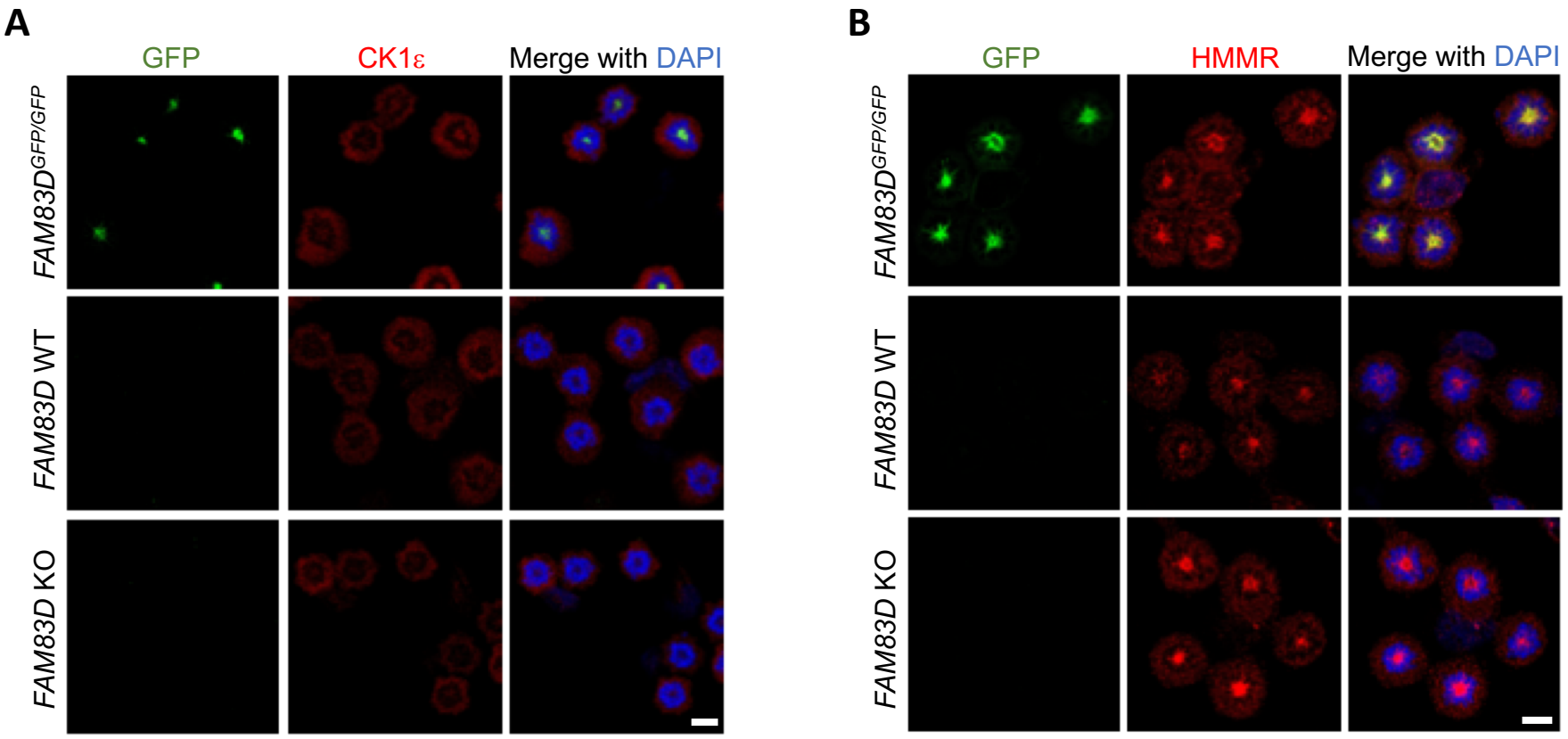
A
GFP
CK1ε
Merge with DAPI
FAM83D GFP/GFP
FAM83D WT
FAM83D KO
B
GFP
HMMR
Merge with DAPI
FAM83D GFP/GFP
FAM83D WT
FAM83D KO

Figure EV2

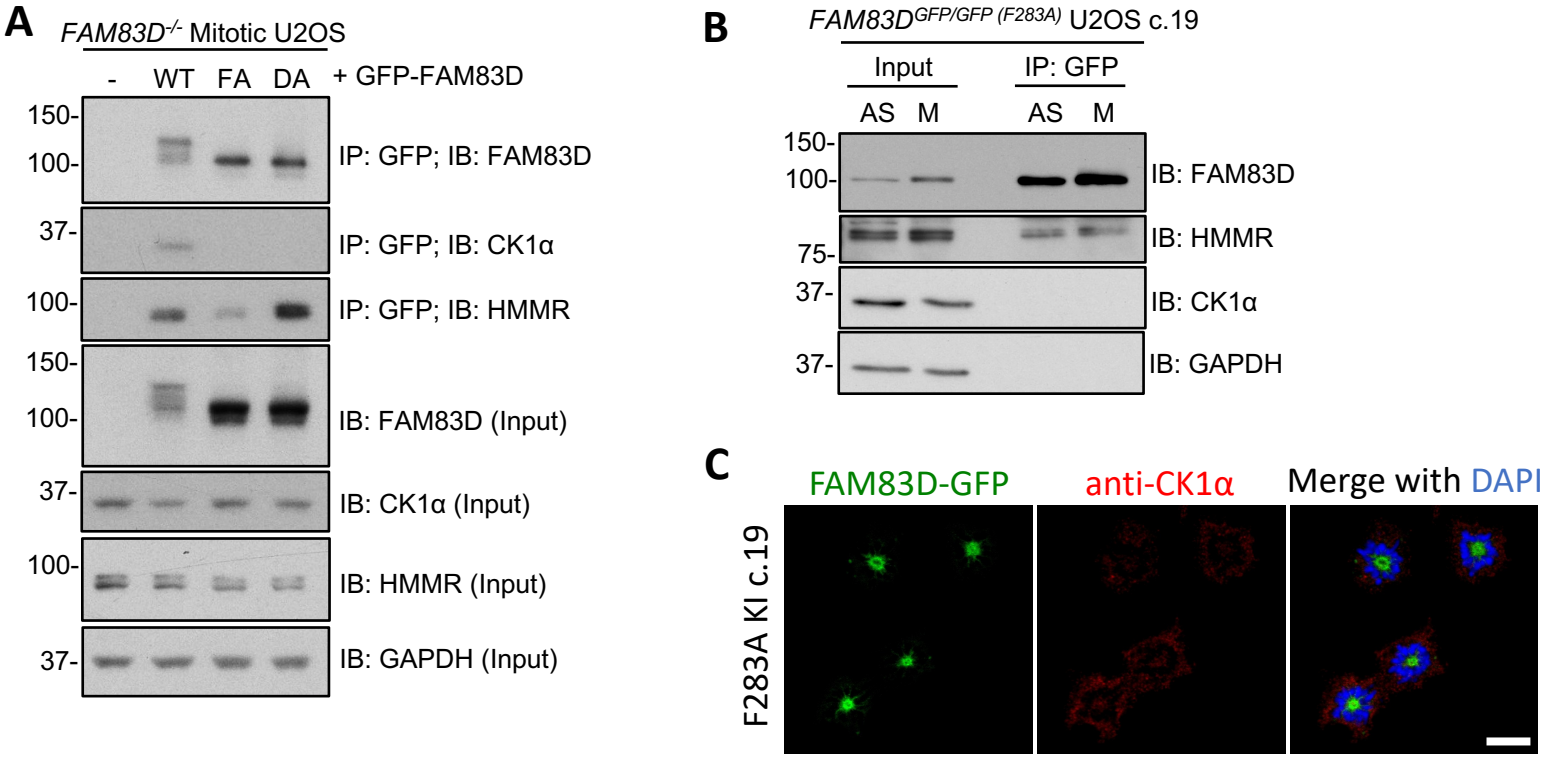
A
FAM83D-/- Mitotic U2OS
- WT FA DA + GFP-FAM83D
150-
100-
IP: GFP; IB: FAM83D
37-
IP: GFP; IB: CK1α
100-
IP: GFP; IB: HMMR
150-
100-
IB: FAM83D (Input)
37-
IB: CK1α (Input)
100-
IB: HMMR (Input)
37-
IB: GAPDH (Input)
B
FAM83DGFP/GFP (F283A) U2OS c.19
Input
IP: GFP
AS M AS M
150-
100-
IB: FAM83D
75-
IB: HMMR
37-
IB: CK1α
37-
IB: GAPDH
C
FAM83D-GFP
anti-CK1α
Merge with DAPI
F283A KI c.19

Figure EV3

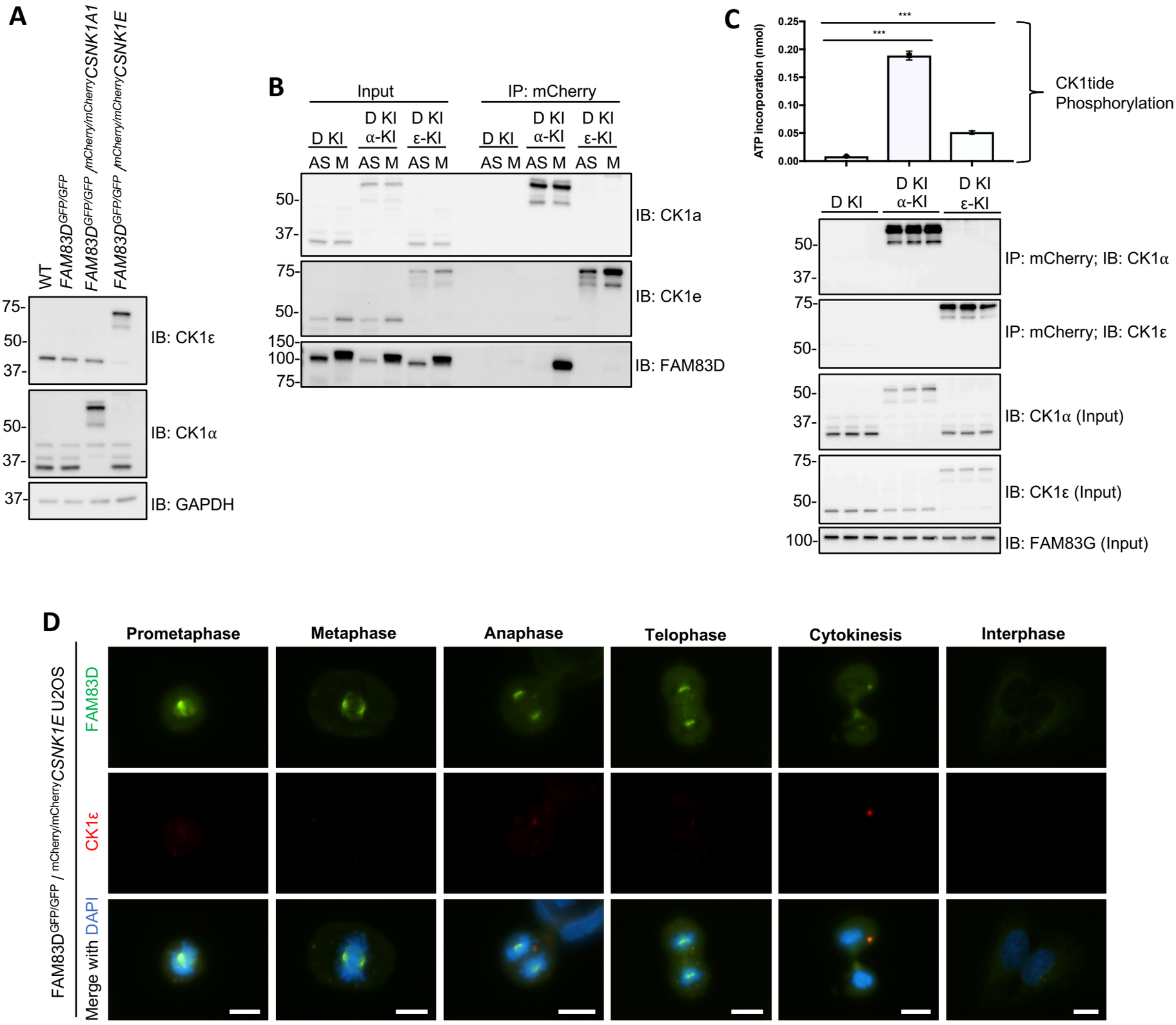
A
WT
FAM83D GFP/GFP
FAM83D GFP/GFP /mCherry/mCherry CSNK1A1
FAM83D GFP/GFP /mCherry/mCherry CSNK1E
75-
50-
37-
IB: CK1ε
50-
37-
IB: CK1α
37-
IB: GAPDH
B
Input
IP: mCherry
D KI
D KI α-KI
D KI ε-KI
AS M AS M AS M AS M AS M AS M
50-
37-
IB: CK1a
75-
50-
IB: CK1e
150-
100-
75-
IB: FAM83D
C
ATP incorporation (nmol)
0.25
0.20
0.15
0.10
0.05
0.00
***
***
CK1tide Phosphorylation
D KI
D KI α-KI
D KI ε-KI
50-
37-
IP: mCherry; IB: CK1α
75-
50-
IP: mCherry; IB: CK1ε
50-
37-
IB: CK1α (Input)
75-
50-
IB: CK1ε (Input)
100-
IB: FAM83G (Input)
D
Prometaphase
Metaphase
Anaphase
Telophase
Cytokinesis
Interphase
FAM83D GFP/GFP / mCherry/mCherry CSNK1E U2OS
FAM83D
CK1ε
Merge with DAPI

Figure EV4

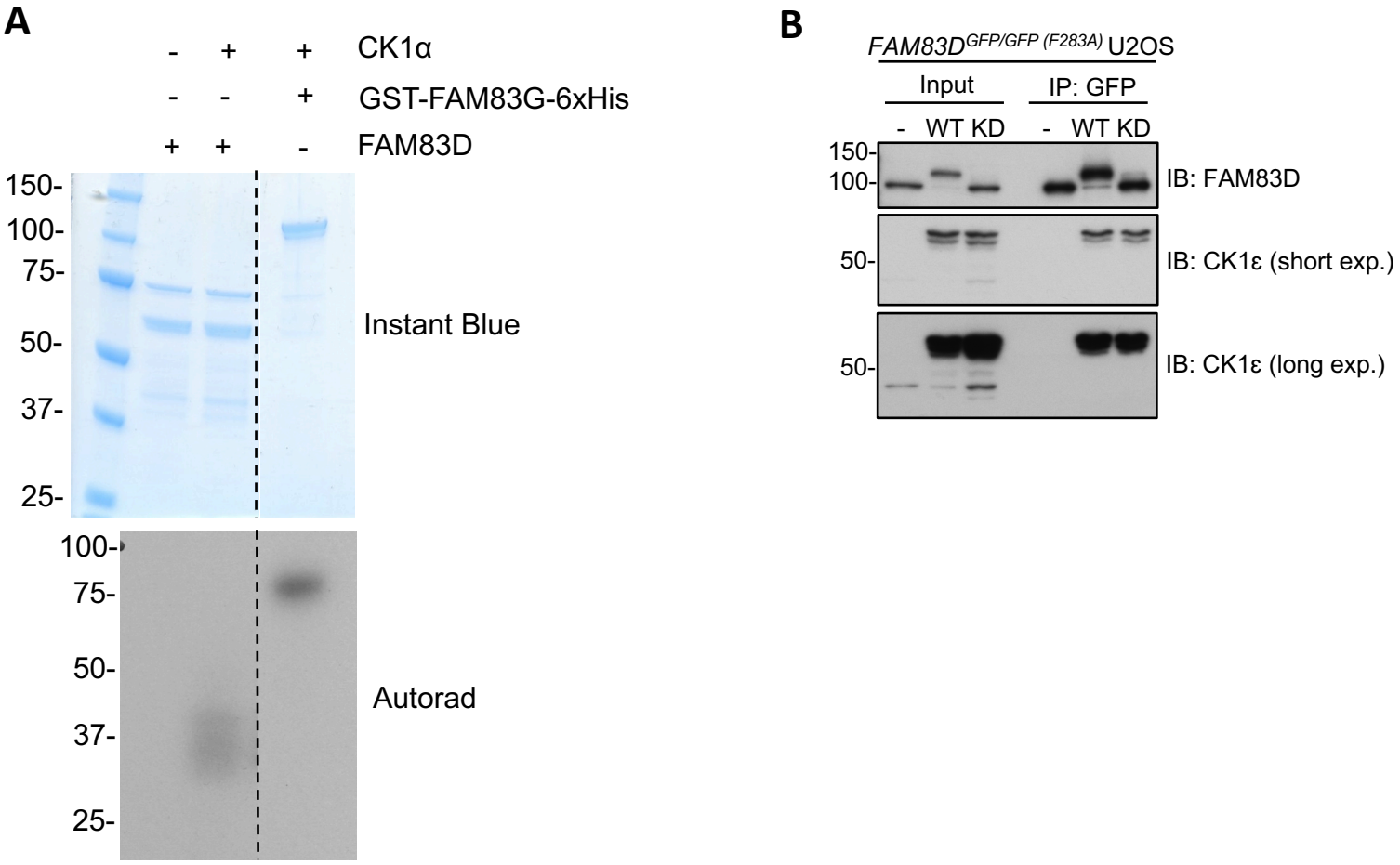
A
- + + CK1α
- - + GST-FAM83G-6xHis
+ + - FAM83D
150-
100-
75-
50-
37-
25-
Instant Blue
100-
75-
50-
37-
25-
Autorad
B
FAM83D GFP/GFP (F283A) U2OS
Input
IP: GFP
- WT KD - WT KD
150-
100-
IB: FAM83D
50-
IB: CK1ε (short exp.)
50-
IB: CK1ε (long exp.)

Figure EV5

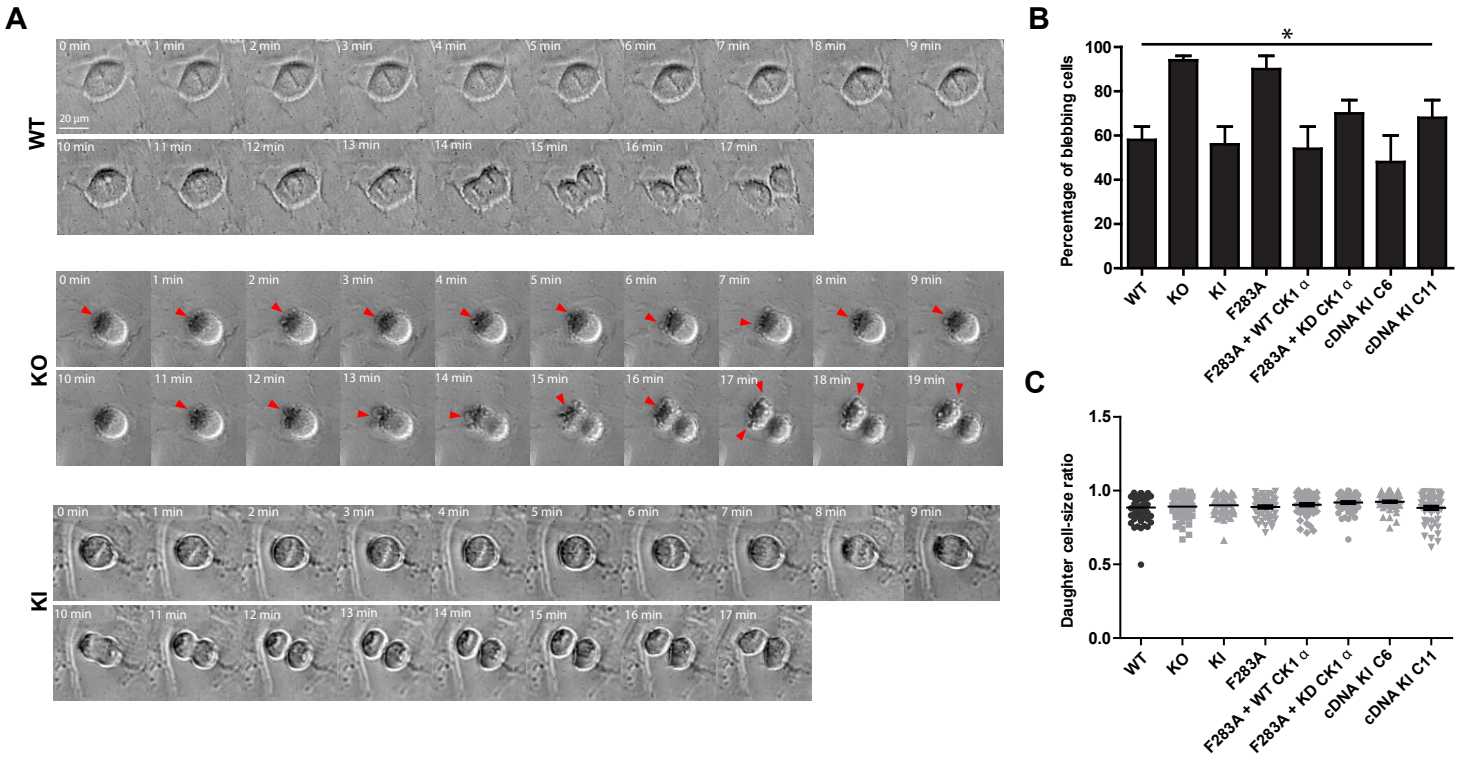
A
WT
KO
KI
0 min
1 min
2 min
3 min
4 min
5 min
6 min
7 min
8 min
9 min
10 min
11 min
12 min
13 min
14 min
15 min
16 min
17 min
18 min
19 min
20 µm
B
Percentage of blebbing cells
100
80
60
40
20
0
*
WT
KO
KI
F283A
F283A + WT CK1 α
F283A + KD CK1 α
cDNA KI C6
cDNA KI C11
C
Daughter cell-size ratio
1.5
1.0
0.5
0.0

Figure EV6

```
// Spindle stain quantification macro
// - measure stain in spindle region bounded by DAPI ring exterior
// - measure stain outside DAPI ring region to estimate background
// - for each nucleus identified, report ratio spindle/background
//
// for Luke Fulcher, 2018
//
// Copyright Graeme Ball 2018, Dundee Imaging Facility
// License: Creative Commons CC-BY-NC-SA
//

// parameters
chDAPI = 3;  // channel number for DAPI
chCK1a = 1;  // channel for CK1alpha stain
minSizeSpindle = 8000;  // minimum number of pixels in a spindle
region
Dialog.create("Measure_spindle_ratio");
Dialog.addNumber("DAPI channel", chDAPI);
Dialog.addNumber("CK1a channel", chCK1a);
Dialog.show();
chDAPI = Dialog.getNumber();
chCK1a = Dialog.getNumber();

roiManager("reset");
roiManager("UseNames", "true");
roiManager("Show All with labels");
run("Set Measurements...", "area mean standard min integrated
display redirect=None decimal=3");
setOption("BlackBackground", true);

// find spindle regions
Stack.setDisplayMode("grayscale");
Stack.setChannel(chDAPI);
run("Duplicate...", " ");
run("Convert to Mask", "method=Otsu background=Dark calculate
black");
run("Fill Holes");
run("Analyze Particles...", "size=" + minSizeSpindle + "-Infinity
exclude add");
close();

// create CK1a whole-cell mask with separated cells
Stack.setChannel(chCK1a);
run("Duplicate...", " ");
setAutoThreshold("Triangle dark");
run("Convert to Mask");
run("Fill Holes");
run("Median...", "radius=15");  // clean up rough edges
run("Make Binary");
run("Watershed");

// for each spindle ROI, attempt to find containing cell ROI and
create cytoplasm ring ROI
nNuclei = roiManager("count");
```

```
setThreshold(1, 255);
for (i = 0; i < nNuclei; i++) {
        roiManager("select", i);
        roiManager("rename", "spindle" + i);
        getSelectionBounds(x, y, w, h);
        x = round(x + w/2);
        y = round(y + h/2);
        doWand(x, y);
        roiManager("add");  // cytoplasm region centred on this
spindle
        newCellIndex = roiManager("count") - 1;
        indices = newArray(i, newCellIndex);
        roiManager("select", indices);
        roiManager("XOR");
        roiManager("add");
        newCytoIndex = roiManager("count") - 1;
        roiManager("select", newCytoIndex);
        roiManager("rename", "cytoplasm" + i);
        roiManager("select", newCellIndex);
        roiManager("delete");
}
close(); // close CK1a whole-cell mask

// make measurements using paired ROIs and write to Results table
run("Clear Results");
Stack.setChannel(chCK1a);
for (i = 0; i < nNuclei; i++) {
        row = nResults;
        setResult("cellID", row, i);
        roiManager("select", i);
        getRawStatistics(nPixels, spMean, min, max, std);
        setResult("spindleMean", row, spMean);
        setResult("spindleTotal", row, (spMean * nPixels));
        roiManager("select", i + nNuclei);  // corresponding
cytoplasm ROI
        getRawStatistics(nPixels, cyMean, min, max, std);
        setResult("cytoMean", row, cyMean);
        setResult("ratioS/C", row, (spMean/cyMean));
}

//run("From ROI Manager");
```